



Cite this: *Nanoscale*, 2018, **10**, 17477

Fabrication and application of BN nanoparticles, nanosheets and their nanohybrids

Dmitry V. Shtansky, ^{*a} Konstantin L. Firestein^b and Dmitri V. Golberg ^{*b,c}

Smart implementation of novel advanced nanomaterials is the key for the solution of many complex problems of modern science. In recent years, there has been a great interest in the synthesis and application of boron nitride (BN) nanotubes because of their unique physical, chemical, and mechanical properties. By contrast, the synthesis, characterization and exploration of other morphological types of BN nanostructure – BN nanoparticles and BN nanosheets – have received less attention. However, the detailed investigations on advantages of every morphological BN type for specific applications have only recently been started. One of the promising directions is the utilization of BN-based nanohybrids. This review is dedicated to the in-depth analysis of recently published works on the fabrication and application of BN nanoparticles, nanosheets, and their nanohybrids. It covers a variety of developed synthetic methods toward fabrication of such nanostructures, and their specific application potentials in catalysis, drug delivery, tribology and structural materials. Finally, the review focuses on the theoretical aspects of this quickly emerging field.

Received 21st June 2018,
 Accepted 10th September 2018
 DOI: 10.1039/c8nr05027a
rsc.li/nanoscale

^aNational University of Science and Technology "MISIS", Leninsky prospect 4, Moscow, 119049, Russian Federation. E-mail: shtansky@shs.misis.ru
^bScience and Engineering Faculty, Queensland University of Technology, 2nd George St., Brisbane, QLD 4000, Australia. E-mail: dmitry.golberg@qut.edu.au
^cWorld Premier International Center for Materials Nanoarchitectonics (WPI-MANA), National Institute for Materials Science (NIMS), Tsukuba, Namiki 1, Ibaraki 3050044, Japan



Dmitry V. Shtansky

Dmitry V. Shtansky is head of the Laboratory of Inorganic Nanomaterials, Professor at the Department of Powder Metallurgy and Functional Coatings and Principal Scientists at the Scientific-Educational Center of SHS. He graduated from the Physics Department of Moscow State University (1985) and received a Ph.D. at the I.P. Bardin Iron and Steel Industry Institute (1992) and a Doctor of Science degree at the National University of Science and Technology "MISIS" (2002). The field of his scientific interest includes but is not limited to BN nanostructures, composite materials, biomaterials, catalysts, thin films and coatings, surface engineering, and nanostructured and nano-composite materials.

1. Introduction

Layered nano-boron nitride (BN) is attracting huge interest and is a promising material for various applications as a catalyst, antibacterial agent, surface enhanced Raman spectroscopy (SERS) substrate; nanocarrier for drug-delivery; boron neutron capture therapy agent; solid lubricant; nanofiller-like



Konstantin L. Firestein

Konstantin L. Firestein after obtaining his PhD at the National University of Science and Technology "MISIS" (Moscow, Russia), Konstantin L. Firestein became a staff member in Professor Golberg's group at Queensland University of Technology (Brisbane, Australia). His main research topics are CVD synthesis of various nanomaterials, mechanical properties of various nanostructures and composite

materials (for example Al-BN composites) and studying the catalytic activity of BN-based nanohybrids.

reinforcing phase in metallic-matrix and polymer-matrix composites (MMCs and PMCs); water purifier, gas and biological sensor; photodetector; and an element of electronic, plasmonic, optoelectronic, semiconducting, and magnetic devices. Such a wide range of applications is associated with its unique combination of physical and chemical properties, such as low specific density, high thermal stability, oxidation resistance, excellent dispersion stability and transparency, larger interlayer shear force (compared with its famous counterpart – graphene), enhanced adsorbing capacity, and a wide band gap. The interest in this field is rapidly growing; for example for the past ten years the number of related citations (*e.g.* the search keywords “BN-nanosheets”, “BN-nanoparticles”, and “BN-nanocomposites”) grew more than eightfold, as confirmed by the statistics presented by the *Scopus* database (Fig. 1).

Nano-BN advanced applications are truly diverse. For instance, Li *et al.*¹ used as-prepared freestanding BN nanosheet films and confirmed their outstanding hydrophobicity and lipophilicity properties. Such specific features make them applicable in oil/water separation with very high fluxes, up to $1\,200\,000\text{ L m}^{-2}\text{ h}^{-1}\text{ bar}^{-1}$, and excellent separation efficiencies (ppm level in terms of the water content in the filtrate). Xue *et al.*² was able to arrange BN nanosheet-interconnected 3D frameworks with high porosity and embedded them into a PMMA polymer. The composites revealed combinatorial multi-functional properties, such as excellent mechanical strength, light weight, ultralow coefficient of thermal expansion, highly isotropic thermal conductivities ($\approx 26\text{--}51$ multiples of pristine polymer), low dielectric constants, super-low dielectric losses, and high resistance to softening at elevated temperatures. Importantly, the regarded 3D-BN frameworks were easily recycled from their polymer composites, and may be reliably utilized for reuse. These materials were found to be highly valuable for new-era advanced electronic packaging. He *et al.* demonstrated that BN nanosheets may nicely function as

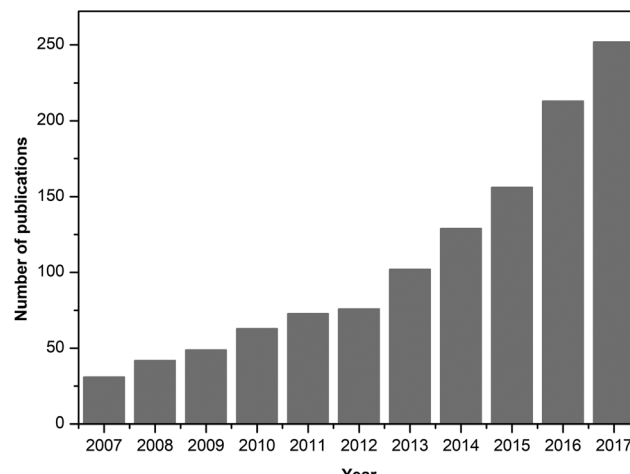


Fig. 1 Statistics of publication activity on nano-BN materials while using “BN-nanosheets”, “BN-nanoparticles”, and “BN-nanocomposites” as keywords for the search. The data is from Scopus as of Aug. 29, 2018.

effective photocatalyst supports for H_2 production once they are paired with standard TiO_2 photocatalysts.³ Such hybrids markedly enhanced light absorption, significantly retarded charge pair recombination, facilitated interfacial electron transfer, and lowered interfacial charge transfer resistance. As a result, the photocatalytic H_2 production activity of $\text{TiO}_2@\text{BN}$ composites, which consisted of only earth-abundant elements, was comparable to that of conventional and expensive Pt– TiO_2 . In many cases, BN nanosheet-containing hybrids may also be effectively used for effective removal of heavy metal ions⁴ and on-demand adsorption of various species.^{5,6} BN nanosheets containing waterborne polyurethane coatings demonstrated significantly improved corrosion resistance and antifriction properties.⁷ BN nanoflakes with modulated band-gaps were effectively applied for UV photodetection.⁸ And BN nanoparticles may be added into engine oils for affecting its pressure properties⁹ or be used for decoration of carbon nanomaterials employed for hydrogen storage.¹⁰ These and many other smart applications of BN nanosheets, nanoparticle and there hybrids are in detail described in the following sections.



Dmitri Golberg

Dmitri Golberg is a Professor of Queensland University of Technology (QUT), Australia, and an Australian Research Council Laureate Fellow. He joined QUT in 2017 after 20 years of his career in Japan, where he held the positions of a Nanotube Group Leader of the National Institute for Materials Science (NIMS), Tsukuba, and a Professor of University of Tsukuba. He is a recipient of many prestigious awards, e.g.

Tsukuba Prize (2005), Thomson Reuters Research Front Award (2012), “Seto” Prize by Japan Microscopy Society (2016), and NIMS President Award (2017). Dmitri is a 2014–2018 Highly Cited Researcher in Materials Science (Clarivate Analytics).

2. Synthesis of BN nanostructures

BN nanostructures can be fabricated in different structural types and morphologies: quantum dots (zero-dimensional (0D)), nanotubes (one dimensional (1D)), graphene-like BN (two-dimensional (2D)), and various three-dimensional (3D) configurations. Nanowires, nanoribbons, nanofibers, nanospheres, nanocages, nanocones, nano-polyhedra, and nanosheets were all reported, Fig. 2. Extensive information on the synthesis of various BN morphologies can be found in recent papers. Comprehensive reviews of available data related to the synthesis of 2D hexagonal BN (*h*-BN) were recently presented by Zhang *et al.*¹¹ and Kalay *et al.*¹² The fabrication methods included mechanical, liquid, and ion-intercalation

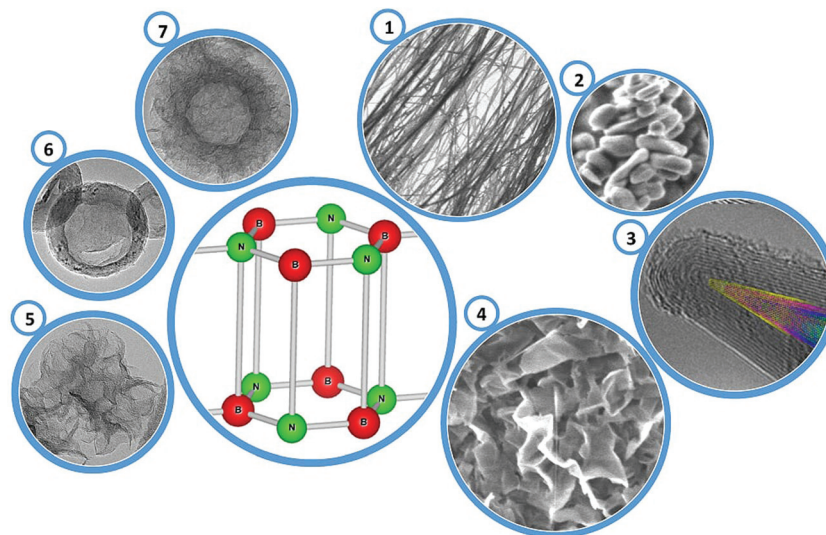


Fig. 2 Atomic structure of a hexagonal boron nitride and microscopic images of diverse BN nanostructures reported till now. (1) – Nanotubes; (2) – nanoparticles; (3) – nanocones; (4) – graphene-like petals; (5, 6, 7) – nanospheres of different morphology.

assisted exfoliations, chemical and physical vapor depositions (CVD and PVD), pulsed laser deposition, unzipping of BN nanotubes, pyrolysis, and surface segregation-based methods. Synthetic routes toward the fabrication of BN monolayers, multilayers, nanomeshes, nanowaves, nanoflakes, nanosheets and nanoribbons were considered by Pakdel *et al.*¹³ Recent advancements in the synthesis of BN nanoparticles (BNNPs) by spray-pyrolysis of borazine were reviewed by Salles and Bernard.¹⁴

Understanding physical background behind the growth mechanisms is essential to achieve large-scale and reproducible synthesis of desirable BN morphology. For example, it was found that various BN nanostructures grow during reactions of alkali and alkaline earth metal borates with ammonia depending on borate composition and synthesis temperature.¹⁵ The type of morphology and yield of BN nanostructures depended on basicity of a metal oxide and its fraction in a precursor borate.

For many practical applications (*i.e.* catalysis, lubrication and drug delivery), spherical shape of BNNPs are of particular interest. Spherical *h*-BNNPs with an average size of 20 nm, a large surface area of $145 \text{ m}^2 \text{ g}^{-1}$ and a total pore volume of $0.41 \text{ cm}^3 \text{ g}^{-1}$ were synthesized by a two-stage (spray drying and pyrolysis) technology.¹⁶ Application of spray drying was shown to be essential for the uniformity of highly dispersible BNNPs. Larger spherical BNNPs with outer diameter of $0.3\text{--}1 \mu\text{m}$ and approximately 3.5 nm pore size were fabricated using boron acid and urea as the precursors by temperature-controlled pyrolysis in a N_2 atmosphere.¹⁷ Nanoparticles (NPs) usually suffer from the strong tendency for agglomeration. In order to increase long-term stability of *h*-BN aqueous solutions, BNNPs were doped with oxygen.¹⁸ High oxygen content on the surface of BN nanospheres can increase the particle charge hereby improving their dispersion and stability in water at high concentrations. Such BNNPs were fabricated by using boric acid

and melamine as raw materials and hydrothermal carbon spheres as the hard template.¹⁸ To uncover the origin of room-temperature ferromagnetism in BN due to oxygen doping, Lu *et al.*¹⁹ synthesized BNO NPs *via* the reaction of ammonia gas and boric acid. Six types of spherical oxygen-contained BNNPs with hollow and solid cores and smooth and petalled surfaces (with numerous thin-walled BN petals) were synthesized using a CVD route from three types of precursors, *i.e.* $\text{FeO} + \text{MgO} + \text{B}$, $\text{SnO} + \text{MgO} + \text{B}$ and $\text{H}_3\text{BO}_3 + \text{MgO} + \text{B}$.²⁰ Changing the experimental conditions was shown to affect the particle morphology, oxygen content, and the product yield.

Great attention was also paid to the synthesis of flat BN morphologies (flakes and nanosheets), because they are ideally suited as templates and supports to form assemblies for chemical/biochemical applications, electronic devices and composite materials. For example, *h*-BN flakes were synthesized through combining low temperature combustion synthesis and carbothermal reduction and nitridation methods. They were shown to be a promising material for electrochemical detection of ascorbic acid, dopamine and uric acid.²¹ Hexagonal/turbostratic BN nanosheets (BNNSs) with lateral size of tens of micrometers and thickness of tens of nanometers were obtained *via* a facile chemical foaming process at 1400°C utilizing ammonia borane as a precursor.²² A biomass-inspired strategy for synthesizing highly crystalline and purified hexagonal BNNSs using ambient pressure CVD using *bel-lamya quadrata* shells as the raw material was proposed by Geng *et al.*²³ Post-synthesis high-temperature treatment is a powerful tool to change the surface chemistry and to endow nanoparticles with new functional properties. Liang *et al.*²⁴ demonstrated that annealing in Ar or NH_3 in the range of $1400\text{--}1600^\circ\text{C}$ led to the formation of nitrogen vacancies on the surface of BN nanospheres and grafting of the $-\text{NH}_4^+$ functional groups.

3. Synthesis of metal/BN nanohybrids

3.1 Noble metal/BN nanohybrids

Noble metals are commonly used to fabricate metal/BN nanohybrids (NHs) with either spherical or flat BN morphologies for advanced catalysts, photocatalysts, molecule probe sensors, SERS substrates, and antibacterial agents. Spherical Ag/BN NHs with petal-like surfaces were fabricated using two different methods: CVD of BNNPs in the presence of Ag vapours, and ultraviolet decomposition of AgNO_3 in a suspension of BNNPs.²⁵ Depending on the method, the NHs revealed different structure. Since, during the CVD process, the formation of Ag NPs occurred simultaneously with the growth of BN petals, the major part of Ag NPs was covered with the layers of *h*-BN. In contrast, during UV decomposition of AgNO_3 , Ag NPs were nucleated on the surface of BNNPs and, therefore, remained free from the *h*-BN shells. Ag/BN NHs were also prepared by Ag ion implantation into hollow BNNPs with a petal-like surface (Fig. 3a and b).²⁶ By adjusting ion energy, it was possible to control the number of defects and a volume fraction of amorphous BN phase, thereby opening new

opportunities for creating hybrid materials with specific band gap, as well as optoelectronic and photovoltaic devices. Nanocomposites composed of Ag NPs deposited onto *h*-BN layers were fabricated by microwave assisted method and studied by Gao *et al.*²⁷ The results indicated that the formation of Ag/BN NHs occurred mainly *via* physical adsorption and electrostatic interaction. Several wet chemistry methods were employed to fabricate noble metal/BN NHs. For example, Ag/BNNPs NHs with different amounts of boron oxide on their surfaces were produced *via* ultraviolet decomposition of AgNO_3 in a mixture of polyethylene glycol and BNNPs.²⁵ BN nanospheres decorated with noble metal NPs (Au, Pt, Pd, Ag) were prepared *in situ* by adding corresponding salts (HAuCl_4 , PdCl_2 , H_2PtCl_6 , AgNO_3) into a BN nanosheet dispersion.²⁸ Shen *et al.*²⁹ suggested a low cost and eco-friendly strategy to fabricate Ag NPs/BN nanosheet hybrids in aqueous solution, without additional reductants or heating. BN nanosheets were modified with a thin layer of tannic acid–ferric ion (TA–Fe) complex to graft Ag NPs through reduction of tannic acid. Au/BN nanosheet hybrids were also obtained using the Lewis base interaction with hydrophilic chains of amine-functionalized

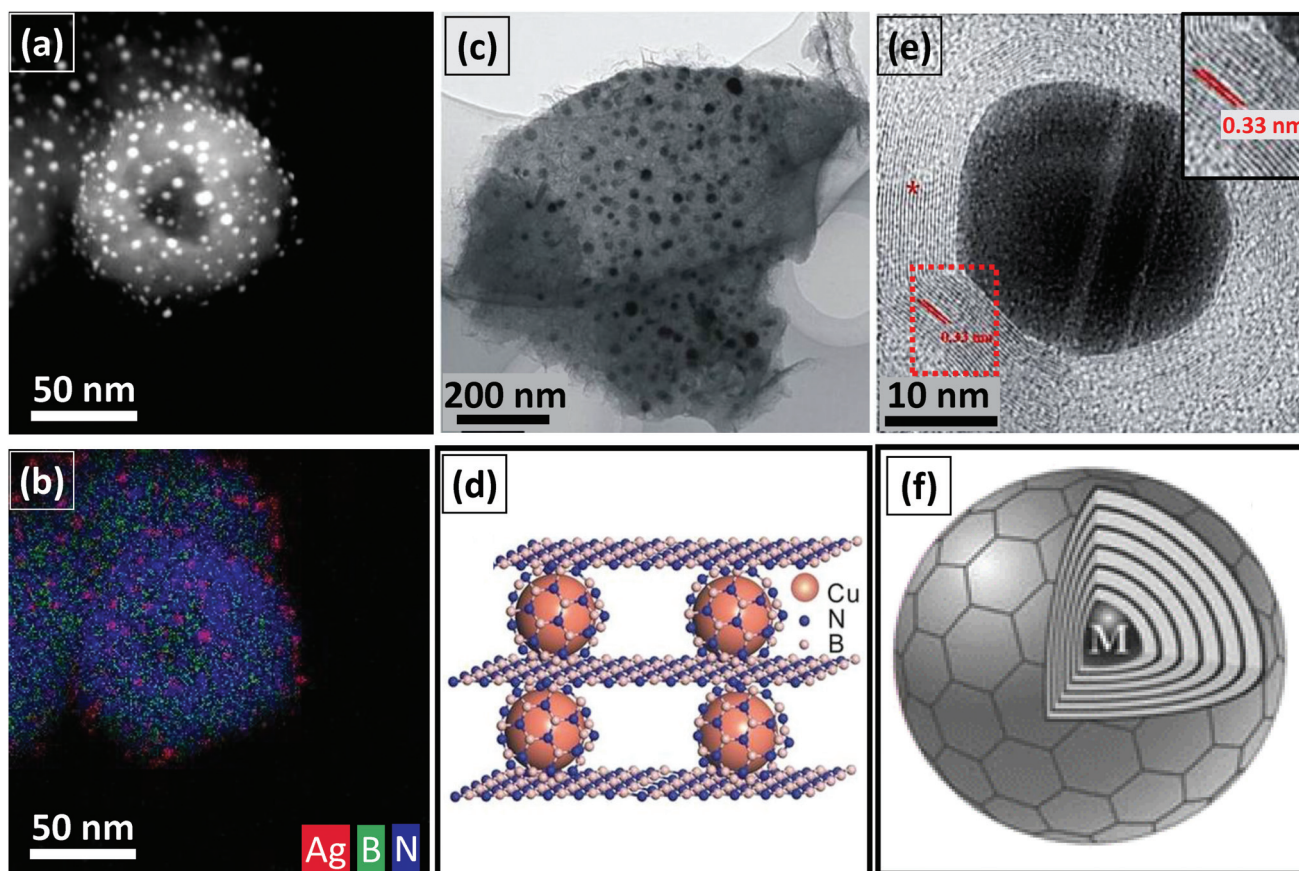


Fig. 3 (a) HAADF-STEM image and (b) corresponding spatially-resolved EDX map of Ag/BN NHs prepared by Ag ion implantation into hollow BNNPs with a petal-like surface;²⁶ (c) TEM image and (d) schematic architecture of Cu/BN NHs prepared *via* one-step thermal decomposition;³¹ (e) HRTEM image and (f) a 3D structural model of a BN sphere with the Ni NP core;³⁴ (a) and (b) reprinted with permission from ref. 26. Copyright 2015, Elsevier. (c) and (d) Reprinted with permission from ref. 31. Copyright 2015, Springer Nature. (e) and (f) reprinted with permission from ref. 34. Copyright 2013, Royal Society of Chemistry.

Au NPs forming complexes with the electron-deficient boron atoms on *h*-BN.³⁰

3.2 Metal/BN core–shell nanohybrids

Another sub-direction in the field of metal/BN NHs is fabrication of core–shell particles. *h*-BN encapsulated Cu NPs were prepared *via* one-step thermal decomposition (Fig. 3c and d).³¹ Due to the encapsulation by *h*-BN, the Cu NPs remained very stable in air at room temperature without any obvious oxidation. Bimetallic CoNi NPs encapsulated within *h*-BN (CoNi@*h*-BN), as prospective catalytic dehydrogenation nanoreactors, were synthesized *via* annealing of freshly prepared metal ammine boride complexes [Co_{0.5}Ni_{0.5}(NH₃)₆]Cl₃/NH₄BO₂ and KBH₄ under flowing nitrogen gas at 900 °C.³² CoNi NPs, 5–25 nm in size, were completely encapsulated by 10–20 layers of *h*-BN shells. Fe₃O₄ NPs-coated BN nanospheres (Fe₃O₄@BNNS) were obtained *via* ethanol-thermal method for potential application in water treatment, catalysts, carriers for boron neutron capture therapy and magnetic-targeted drug delivery.³³ Spherical BN nanospheres were preliminary synthesized using a carbon-free CVD method from trimethoxyborane (B(OMe)₃) and ammonia as reactants. Ferrocene and nickelocene were added to borazine to improve the crystallization of core–shell BNNPs.³⁴ Fe@*h*-BN and Ni@*h*-BN NPs, fabricated at 1200 °C, demonstrated a higher order of crystallization than nanohybrids obtained at 1600 °C without metal additives (Fig. 3e and f).

4. BN-based nanohybrids as promising catalysts

Catalyst nanohybrid development is based on the right selection of both nanocarriers and catalyst agents. Catalysts in the powder form usually suffer from the strong tendency for agglomeration and impossibility of multiple usages after complex recycling, which significantly limits their practical applications. Due to their high surface area, thermal and chemical stability BN nanospheres and graphene-like nanosheets are promising platforms for supporting metal and oxide NPs in high-performance heterogeneous catalysts and photocatalysts. The support can influence: (i) the dispersion of the active material and its thermal stability by forming chemical surface bonds, which prevent coarsening of the active nanoparticles, (ii) the catalytic activity of the active material through the polarization of electronic bonds, and (iii) various chemical reactions (promoting or inhibiting them). Unlike graphite, BN has unshared electron pairs localized on the nitrogen atoms, resulting in a polarized nature. In addition, the electronic properties of 2D *h*-BN very strongly depend on impurities: in fact, surface doping with hydrogen or fluorine was reported to significantly reduce the bandgap and the material can become a semimetal.^{35,36} Utilization of *h*-BN support can improve the photocatalytic performance of the bulk semiconductors by promoting the separation of electrons and holes in the photocatalytic reaction. Moreover, the theore-

tical calculations and experimental verifications demonstrated that defective BNNS better immobilized metal nanoparticles and achieved higher catalytic activities in comparison with defect-free *h*-BN.^{37–41} A first-principles calculations showed that Cu atoms strongly interact with *h*-BN surface defects, which prevent their aggregation.⁴² In addition, Cu atoms embedded in the BN surface effectively activate CO molecules, which allows one to consider such system as a potentially effective catalyst for the oxidation of carbon monoxide. The activity of metal nanoparticles on the BNNS surface might be affected by the interaction with the support *via* electron-pushing mechanisms, namely the mixing of the d_{z²} metal orbitals with the N-p_z and B-p_z orbitals of BN layer.^{43,44}

Recently produced heterogeneous catalysts include *h*-BN-supported metal catalysts (Au/BN,^{45,46} Pt/BN,^{47–49} Ag/BN,^{25,50–52} Ni/BN,⁵³ Pd–Fe/BN,⁵⁴ Au–Cu/BN,⁵⁵ etc.), *h*-BN-supported oxide catalysts (Ag₃VO₄/BN,⁷⁷ Ag₃PO₄/BN,^{57,58} WO₃/BN,⁵⁹ etc.), and their combinations, for example Au–TiO₂/BN,^{60,61} *h*-BN-supported porous and mesoporous catalysts (porous TiO₂/BN,^{62,63} mesoSiO₂–Ni/BN⁶⁴), and core–shell nanocatalysts (Cu@BN,³¹ Co@BN,⁶⁵ Ni@BN, CoNi@*h*-BN,³² etc.). These materials find applications in various catalytic reactions, for example, in reduction of oxygen, nitroarenes, and 4-nitrophenol, oxidation of ethanol, methanol conversion, hydrolysis of ammonia borane, thermal decomposition of ammonium perchlorate, hydrogenation of 2,5-dimethylfuran, and others (Fig. 4 and 5). The interaction mechanisms between pollutants and BN-based materials are mainly surface complexation, π–π stacking, and electrostatic interactions.⁶⁶ Another exciting application of the above mentioned NHs is their utilization for degradation of organic contaminants (rhodamine B (RhB), ciprofloxacin, methylene blue (MB), bisphenol A, tetracycline) under visible light illumination. *h*-BN supports are beneficial for enhanced light absorption/emission, charge separation, interfacial electron transfer, low electron–hole recombination, and generation of the active sites on their surfaces. To provide high catalytic activity, small particle size and homogeneous particle distribution over the support surfaces should be obtained. To achieve this goal, appropriate methods of surface functionalization were employed to increase binding affinity.

Several reports indicate catalytic activity of *h*-BN⁶⁷ and C-doped BN⁶⁸ nanostructures. For example, *h*-BN demonstrated remarkable catalytic activity toward oxidative dehydrogenation of propane with a high selectivity for alkenes (~70%). Metal-free photocatalysts, for example C-doped BN semiconductor, can catalyze hydrogen or oxygen evolution from water as well as CO₂ reduction under visible light illumination.⁶⁹

4.1 Nobel metal/BN nanocatalysts

Nobel metal NPs are most used as catalytic agents for BN supports. For example, BNNS decorated with Au NPs were reported to exhibit high catalytic and electrocatalytic activities in the chemical degradation of RhB and electrocatalytic oxidation of hydrazine, respectively.⁴⁶ Ag/BN NHs were also devel-

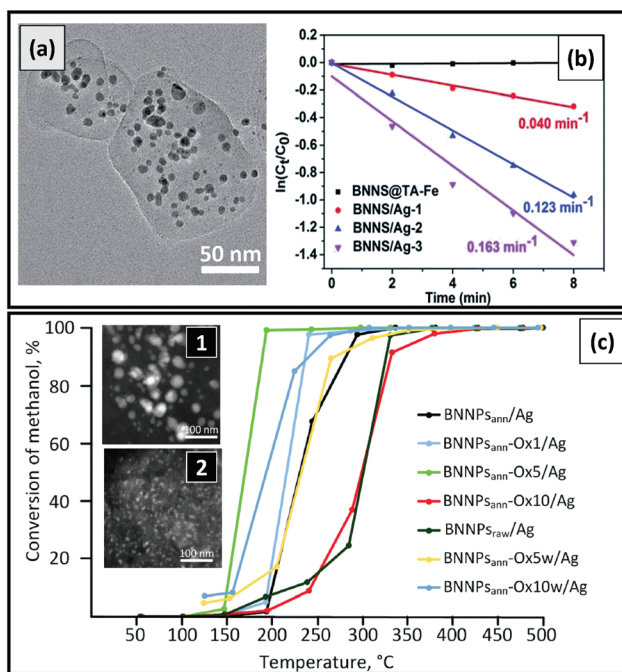


Fig. 4 (a) TEM image of BNNSs covered with Ag NPs and (b) a plot showing the results of catalytic reduction of 4-nitrophenol with Ag/BN NHs as a catalyst;⁵⁰ (c) results of catalytic conversion of methanol by NHs having different amounts of B_2O_3 on the BN surface;⁵¹ insets: STEM-HADF images of Ag/BN NHs prepared using raw BNNPs (1) and BNNPs after air annealing at 1100 °C for 5 min (2).⁵¹ (a) and (b) Reprinted with permission from ref. 50. Copyright 2015, Royal Society of Chemistry. (c) Reprinted with permission from ref. 51. Copyright 2018, Royal Society of Chemistry.

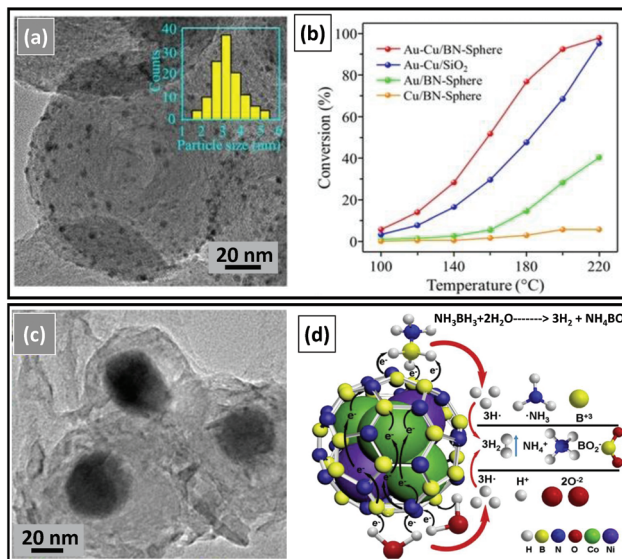


Fig. 5 (a) TEM image of a BN sphere covered with Au–Cu NPs and (b) the results of catalytic oxidation of ethanol with different Me/BN NHs as catalysts;⁵⁵ (c) TEM image of CoNi@h-BN NHs and (d) a scheme of possible reduction mechanism for catalytical hydrolytic dehydrogenation at 293 K.³² (a) and (b) reprinted with permission from ref. 55. Copyright 2017, Wiley. (c) and (d) reprinted with permission from ref. 32. Copyright 2017, Elsevier.

oped and characterized as removing pollution material with high adsorption capacity toward tetracycline (358 mg g^{-1}) and RhB (880 mg g^{-1}).⁷⁰ BNNSs coated with Ag NPs showed superior catalytic activity in reduction of 4-nitrophenol.⁵⁰ Using Ag/BN NHs, 100% methanol conversion at 350 °C was achieved.²⁵ In addition, Ag/BN nanocomposites with encapsulated Ag NPs demonstrated a possibility to create an “eternal catalyst”. The influence of BN surface chemistry on the structure and catalytic activity of Ag/BN NHs was studied by Konopatsky *et al.*⁵¹ It was demonstrated that the presence of B_2O_3 oxide on the BN surface is favorable for Ag NP deposition compared to bare BN surfaces, without oxide. Excessive fraction of B_2O_3 , however, was not beneficial in terms of obtaining the optimal contents of Ag NPs. Pt NP-decorated BN whiskers exhibited a good amperometric response towards the reduction and oxidation of H_2O_2 .⁴⁷ This feature allows them to be used as a smart bioplatform for glucose biosensor. BN-supported Pt catalysts showed the activity toward hydrogenation of 2,5-dimethylfuran.⁴⁸ Contact time study suggested that 2,5-dimethylfuran was hydrogenated *via* two pathways, direct furan ring-opening to 2-hexanone and furan ring-saturation to produce 2,5-dimethyltetrahydrofuran in which the ring-opening was 9-fold faster than the ring-saturation. Ni NPs supported on BN nanospheres and nanosheets were fabricated and were thought to become promising catalysts for hydrogen generation *via* hydrolysis of ammonia borane.⁵³ The NHs showed higher catalytic activity toward hydrogen generation as compared to the unsupported Ni catalyst and retained 83% of its initial catalytic activity after five cycles of ammonia borane hydrolysis. BNNSs were used to anchor bimetallic Pd–Fe NPs in a Pd core–Fe shell configuration. The NHs were highly effective in the heterogeneous catalysis of Suzuki–Miyaura coupling in a benign ethanol–water mixture with yields up to 99% and Pd usage down to 200 ppm.⁵⁴ Spherical BN supported Au–Cu NPs catalysts were fabricated for the low temperature selective oxidation of ethanol.⁵⁵ In such catalysts, Au and Cu were closely coupled species and worked cooperatively to convert ethanol into acetaldehyde. The Au species, containing part of the negative charge on the catalyst surface, contribute to oxygen activation and desorption of acetaldehyde. A catalytic conversion of 77% and selectivity of 94% toward acetaldehyde has been achieved at 180 °C and a high gas hourly space velocity of $100\,000 \text{ mL g}_{\text{cat}}^{-1} \text{ h}^{-1}$. High electrocatalytic activity of Au electrode modified with BNNSs decorated by small Au NPs was also reported and attributed to the oxygen stabilization at Au/BN interface. As a result, the dissociation of OOH^* , an uphill process at BN/Au(111) surface in the 4-electron ORR to H_2O , becomes an energetically favorable downhill process, opening a 4-electron reduction pathway.⁴⁵ BN aerogel comprising of highly crystalline few-layer sp^2 -bonded BNNSs was reported to act as a good catalyst support for Pt NPs.⁴⁹ The Pt/BN aerogel integrated onto a microheater platform allowed for calorimetric propane detection with faster response and shorter recovery time than commonly used alumina support. Fe, Co, and Ni-modified BNNSs were fabricated and studied for ozone molecule removal.⁷¹

4.2 Metal/BN core–shell nanocatalysts

Several recent works were devoted to the synthesis and the evaluation of catalytic activity of metal/BN core–shell nanocatalysts. BN encapsulated Cu NPs exhibited enhanced activity for the thermal decomposition of ammonium perchlorate.⁵¹ The encapsulation by *h*-BN not only stabilized Cu NPs but also maintained their high activity. CoNi@*h*-BN NHs were reported to demonstrate high sustainability, good stability and outstanding catalytic activity toward hydrolysis of ammonia borane under air atmosphere and ambient temperature, compared with their monometallic counterparts.⁵² The activation energy of CoNi@*h*-BN for hydrolysis of ammonia borane was 28 kJ mol⁻¹, which is significantly lower than those reported for various non-noble bimetallic catalysts in the same reaction. It is important that due to enhanced magnetic properties CoNi@*h*-BN NHs can be easily recycled using a magnetic separator. Functionalized *h*-BN were utilized as a stable substance for supporting copper- γ -cyclodextrin complexes (*h*-BN@c-CD@Cu(OAc)₂), serving as a recoverable and reusable catalyst in the multicomponent one-pot synthesis of 1,2,3-triazoles in water.⁵³ This catalyst can be separated easily by filtration and may be used several times in new reactions after recycling. Co@BN core–shell nanocatalysts were utilized for catalytic reduction of nitroarenes to aminoarenes.⁵⁴ The following mechanism for Co@BN catalyzing 4-nitrophenol reduction in the presence of NaBH₄ was proposed: (i) BH₄⁻ are adsorbed on the catalysts surface and transfer electrons to Co NPs to form Co-H species, (ii) electrons are transferred from Co-H species to the adsorbed 4-nitrophenol reducing it to 4-aminophenol, (iii) 4-aminophenol is desorbed from the surface of Co@BN catalysts and dispersed in the reaction solution. *h*-BN supported mesoSiO₂-confined Ni catalyst exhibited excellent catalytic activity and stability (no loss of activity even after 100 h) in the dry reforming of methane.⁵⁵ These characteristics were achieved by a combination of (i) high coke resistance of the *h*-BN support, (ii) confinement effects of mesoSiO₂, (iii) synergistic effects of the nano-sized Ni species and *h*-BN interface in the activation of CH₄ and CO₂ and (iv) strong metal–support interaction.

4.3 Light-driven photocatalysts

Light-driven photocatalysts are of great interest for efficient utilization of solar or ultraviolet light for environmental purification, fuel production, and fine chemical syntheses. Graphene-like *h*-BN was actively used to attain the efficient degradation of pollutants under irradiation. For example, Ag₃PO₄/*h*-BN composites degraded almost all MB under visible-light irradiation within 50 min and its photocatalytic performance didn't show a distinct reduction after five cycling runs.⁵⁶ Introduction of graphene-like *h*-BN to Ag₃PO₄ was shown to significantly improve the separation of photogenerated charge carriers leading to enhanced photocatalytic activity and stability. Ag₃PO₄/BN photocatalysts also showed three times higher photocatalytic degradation of RhB compared with pure Ag₃PO₄.⁵⁷ The presence of BN improves

charge separation ability by suppressing the recombination of photogenerated electron and holes, thereby leaving the possibility of holes in the Ag₃PO₄ NPs participate in the photocatalytic degradation of the organic pollutants which had been adsorbed on the surface of BN. Ag₃VO₄/*h*-BN composites exhibited high photocatalytic activity for the degradation of RhB under visible light compared with pure Ag₃VO₄.⁵⁸ After hybridization, the material absorbance intensity was enhanced both in visible and UV light regions.

WO₃/BN catalysts were demonstrated to show the high photocatalytic activity for ciprofloxacin and RhB under visible light illumination.⁵⁹ The high photocatalytic performance was attributed to the synergistic interactions between WO₃ and BNNSs. WO₃/BN NHs possessed a better adsorption in visible light region, lower electron–hole recombination, higher electron–hole separation and smaller charge transfer resistance than that of the pure graphene-like *h*-BN. Due to the existence of the WO₃/BN interface, the photo-generated electron can transfer from WO₃ to BN and captured by O₂ on the surface of catalyst to generate O₂^{•-} radicals. Simultaneously, the photo-induced holes on the valence band of WO₃ can react with surface-absorbed H₂O or OH⁻ to form the hydroxyl OH·.

Au/TiO₂ particles supported on *h*-BNNSs were fabricated.⁶⁰ Their high photocatalytic activity toward the decomposition of an aqueous organic compound, crystal violet, into CO₂ under solar light irradiation was attributed to three main factors: (i) visible light response caused by Au NPs, (ii) reactant-concentration ability possessed by the BN phase, and (iii) improved charge separation at the TiO₂/BN interfaces. Mixing of Au NPs-loaded TiO₂ photocatalysts with *h*-BNNSs also allowed one to increase oxidative decomposition of formic acid in water under visible light illumination.⁶¹

High catalyst porosity and presence of defects can promote photocatalytic oxidation on the surface by increasing the number of active sites. Oxygen atoms create more active sites, and hence, greatly increase the conductivity of a material compared with that of pristine BN.⁷³ Oxygen-doped BNNSs were reported to be capacitive deionization electrodes for water purification. The ability of NO⁻ groups to coordinate Cd²⁺ explains intensive Cd²⁺ removal from water at a wide range of concentrations.⁷⁴ Singh *et al.*⁶³ reported high specific surface area BN/TiO₂ composites with enhanced photocatalytic activity toward MB degradation under visible light. Compared with pristine TiO₂, BNNSs increased the absorption of absorbents and delayed the recombination rate of electron–hole pairs. Highly active B–O–Ti bonds in porous BN/TiO₂ hybrid nanosheets make them responsive to an extended wavelength range from UV to visible light ($\lambda > 420$ nm) spectrum and also substantially enhance the photocatalytic effect (up to 99%) for degradation of hazardous organic dye (RhB) under visible light.⁶² The successful phenol degradation with porous BN/TiO₂ hybrid nanosheets (38 wt%) further demonstrated their visible-light-driven characteristics. In addition, the porous BN/TiO₂ hybrid nanosheets exhibit excellent cycling stability up to 5 cycles maintaining high visible-light photocatalytic activity (97%).

For the sake of completeness, recently developed graphene-like BN/Bi₄O₅I₂ 2D–2D stacking composites should be mentioned.⁷⁵ They were produced and tested. Their enhanced photocatalytic activity toward degradation of bisphenol A was attributed to the interfacial electron transfer from Bi₄O₅I₂ to graphene-like *h*-BN. Without introducing BNNSs, a fast recombination of photogenerated electron–hole pairs would occur. The presence of *h*-BN can promote the faster interfacial electrons transfer resulting in the activation of the oxygen molecules to produce the O₂^{•-} radical species.

5. BN nanocarriers as advanced drug-delivery and antibacterial systems

Recent studies have confirmed that spherical BNNPs are not toxic.^{76,77} This opens a broad perspective for their utilization as anticancer drug-delivery and antibacterial systems, biological nanovectors and vaccine adjuvants (Fig. 6). Note, however, that the biocompatibility of BNNSs depends on their size, shape, structure, and surface chemical properties. In particular, BNNSs with a size below 1 μm and a thickness less than

100 nm were reported to be less biocompatible as compared to their micrometer-sized counterparts.⁷⁸ It was suggested that unsaturated B atoms located at the nanosheet edges or on the particle surface induce reactive oxygen species (ROS), leading to toxicity.

5.1 BN-based nanocarriers for drug delivery

Excellent adsorbent properties of BNNPs and BNNSs were explored by adsorbing different antibiotics: ciprofloxacin (CIP),⁸⁰ norfloxacin (NOR),⁸⁰ and doxorubicin (DOX)^{76,77} over their surfaces. The adsorption experiments performed at various pH revealed the maximum adsorption at pH 8.4 (DOX) and between 4 and 6 (CIP and NOR).

Recently, an original and simple method aimed at the fabrication of BNNPs with peculiar petal-like surfaces was developed.²⁰ DOX-loaded BNNPs penetrated into the neoplastic IAR-6-1 cells using endocytic pathway and then DOX released into the cytoplasm and cell nuclei resulting in cell death.⁷⁶ The DOX-BN nanoconjugates also demonstrated their high efficiency toward multidrug resistant (MDR) cell lines.⁷⁷ In case of the DOX-BNNPs, the DOX penetration by endocytic mechanism was different from that of the free DOX, hereby allowing for maintaining a high and stable level of DOX in the

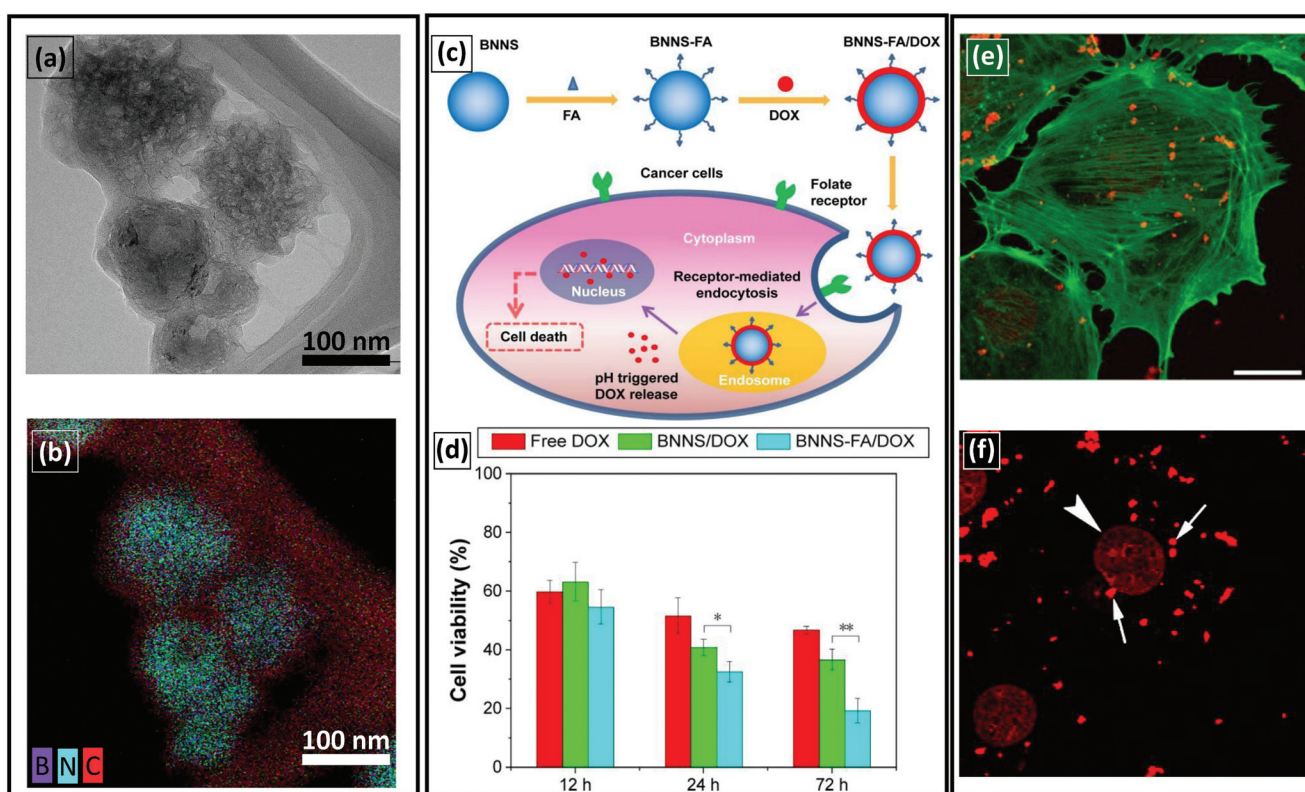


Fig. 6 (a) TEM image of BNNPs loaded with doxorubicin and (b) corresponding spatially-resolved EDX maps showing carbon on BNNPs surface;⁷⁷ (c) scheme of preparation and application of folate-conjugated BN nanospheres for targeted delivery of DOX⁷⁷ and (d) relative viability of HeLa cells incubated with free DOX, BNNPs/DOX complexes and BNNPs-FA/DOX complexes;⁷⁹ (e) Confocal images of BNNPs-DOX in IAR-6-1 neoplastic cells after 7 h of incubation; (f) fluorescence of doxorubicin, BNNPs-DOX complexes are seen near nucleus (arrows);⁷⁶ (a) and (b) reprinted with permission from ref. 77. Copyright 2017 American Chemical Society. (c) and (d) reprinted with permission from ref. 79. Copyright 2016 Feng et al. (e) and (f) Reprinted with permission from ref. 76. Copyright 2015 American Chemical Society.

nuclei of MDR KB-8-5 cells. Permyakova *et al.*⁸¹ took an important follow-up step in developing advanced BNNP-based nanocarriers for targeted drug delivery to tumor cells. The folic acid (FA) molecules were successfully conjugated to BNNPs modified with Ag NPs to provide coupling of FA to BNNPs. Theoretical analysis indicated that the grafting of FA to the surface of BNNPs had not affected FA targeting properties. Folate-conjugated BN nanospheres (BNNS-FA) for targeted delivery of anticancer drugs were also reported by Feng *et al.*⁷⁹ BNNS-FA complexes were fabricated by covalent functionalization of FA onto BNNS *via* esterification reaction and then saturated with DOX. The obtained results indicated that BNNS-FA complexes were nontoxic to HeLa cells up to a high concentration of 100 µg mL⁻¹ and were recognized and specifically internalized by HeLa cells *via* FA receptor-mediated endocytosis. BNNS-FA/DOX complexes exhibited greater cytotoxicity to HeLa cells than free DOX and BNNS/DOX complexes due to the increased cellular uptake of DOX mediated by the FA receptor. Sharker *et al.*⁸² synthesized near infrared (NIR) responsive ICG (I) functionalized *h*-BN as photothermal therapeutic agent (*h*-BNI) and doxorubicin (DOX)-conjugated hyaluronic acid (HA) as tumor targeted chemotherapeutic agent (d-HA-Dox). Using adhesion properties of dopamine (d) the *h*-BNI was integrated with d-HA-DOX to make a tumor targeted photothermal chemotherapeutic agent (*h*-BNI/d-HA-DOX) which effectively damaged cancer cells.

Anticancer therapeutic effect of hollow BNNPs with controlled release of boron for prostate cancer treatment has been demonstrated by Li *et al.*⁸³ Hollow BN spheres induced apoptosis and inhibited the proliferation for both the androgen-sensitive LNCap and androgen-independent DU145 prostate cancer cells. *In vivo* assay demonstrated that hollow BN spheres significantly suppress the tumor occurrence and growth in male BALB/c-nu/nu mice models injected with LNCap prostate cancer cells.

5.2 Antibacterial BN-based nanohybrids

Utilization of BNNPs as supports for bactericidal NPs is one more exciting application of BN nanostructures. It not only increases the colloidal stability of bactericidal NPs but also improves their antibacterial characteristics. For example, Ag/BN NHs with petal-like surfaces were reported to possess a profound antibacterial activity against *Escherichia coli* (*E. coli*) K-261 bacteria.²⁵ Nasr *et al.*⁸⁴ significantly enhanced photocatalytic activity of Ag/TiO₂ composite nanofibers by their mixing with BNNSs. Under visible light, BN-Ag/TiO₂ NHs effectively kill *E. coli* strains and could be used for water disinfection. Water-soluble *h*-BN nanoplates can also act as a reliable biological nanovector to carry proteins by cross-linking immobilization with a typical protein cross-linking reagent.⁸⁵ Another amazing future application of BN nanostructures, which, however, has not yet been widely recognized, is boron neutron capture therapy through selective accumulation of boron compounds in tumor cells followed by their irradiation by a neutron beam.⁸⁶

6. High-strength lightweight metal- and polymer–matrix composites reinforced with BN nanostructures

6.1 Metal–matrix composites

Due to their high mechanical properties BN nanostructures are superb reinforcing agents for lightweight MMCs and PMCs (Fig. 7). Although BNNTs and graphene-like BNNSs demonstrate extremely high tensile strength (approximately 33 and 130 GPa, respectively) and, as it may seem, are ideal reinforcing nanostructures, there are several shortcomings that restrict their wide applications. For example, the synthesis of a large amount of high quality BNNTs and BNNSs is still a challenge. It is also difficult to achieve their homogeneous distribution in a matrix. Taking these considerations into account Firestein *et al.*⁹⁰ utilized commercially-available BNNPs for the fabrication of high-strength Al-based MMCs using spark plasma sintering (SPS) technique. A maximum increase in strength (a 50% increase compared with pristine Al) was observed at 4.5 wt% of BNNPs. In addition, the BN-reinforced composites demonstrated a high value of yield stress (~115 MPa) at 300 °C. Interestingly, BN microparticles were found to be a more preferred additive compared with BNNPs due to the formation of more homogeneous and uniform morphologies within the ball-milled powder mixtures and resultant SPS products.⁹¹ The combination of these two methods was shown to be a promising technique allowing for the formation of reinforcing phases from source materials.⁸⁷ The highest tensile strength of 380 MPa at room temperature and of 170 MPa at 500 °C were obtained for Al/BN composites that were simultaneously reinforced with BN, AlN, and AlB₂ phases. DFT calculations confirmed that the formation of strong Al/AlN and Al/AlB₂ interfaces led to an increase in strength. Interesting result was obtained by Semenic *et al.*⁹² Using high-energy milling of *h*-BN powder for 100 h they obtained powders with 68% of sp³-bonded BN. This material may be of great interest as a filler or reinforcing phase for MMCs.

6.2 Polymer–matrix composites

Wu *et al.*⁹³ mixed BNNPs with epoxy resin to fabricate PMCs. The tensile strength and elongation at break of the composites reached 71.4 MPa and 22.1%, respectively, at 0.4 wt% of BNNPs, that gave an increase of 137% and 146% compared with pure epoxy resin. BNNSs were introduced into plasma sprayed hydroxyapatite coatings to improve their fracture toughness and increase yield strength.⁹⁴

As a filler, BN nanostructures are also suitable for the fabrication of PMCs with enhanced thermal conductivity.^{95–99} Filler orientation along the direction of thermal flow is important to achieve a high thermal conductivity. Recently, a new polymer infiltrating strategy was proposed in which an interstitial space of pre-constructing thermally conductive network was filled with polymer.^{100–102} This method was further improved by combining polymer infiltration with filler diffusion through the polymer to reduce the infiltration time.¹⁰³ Another filler

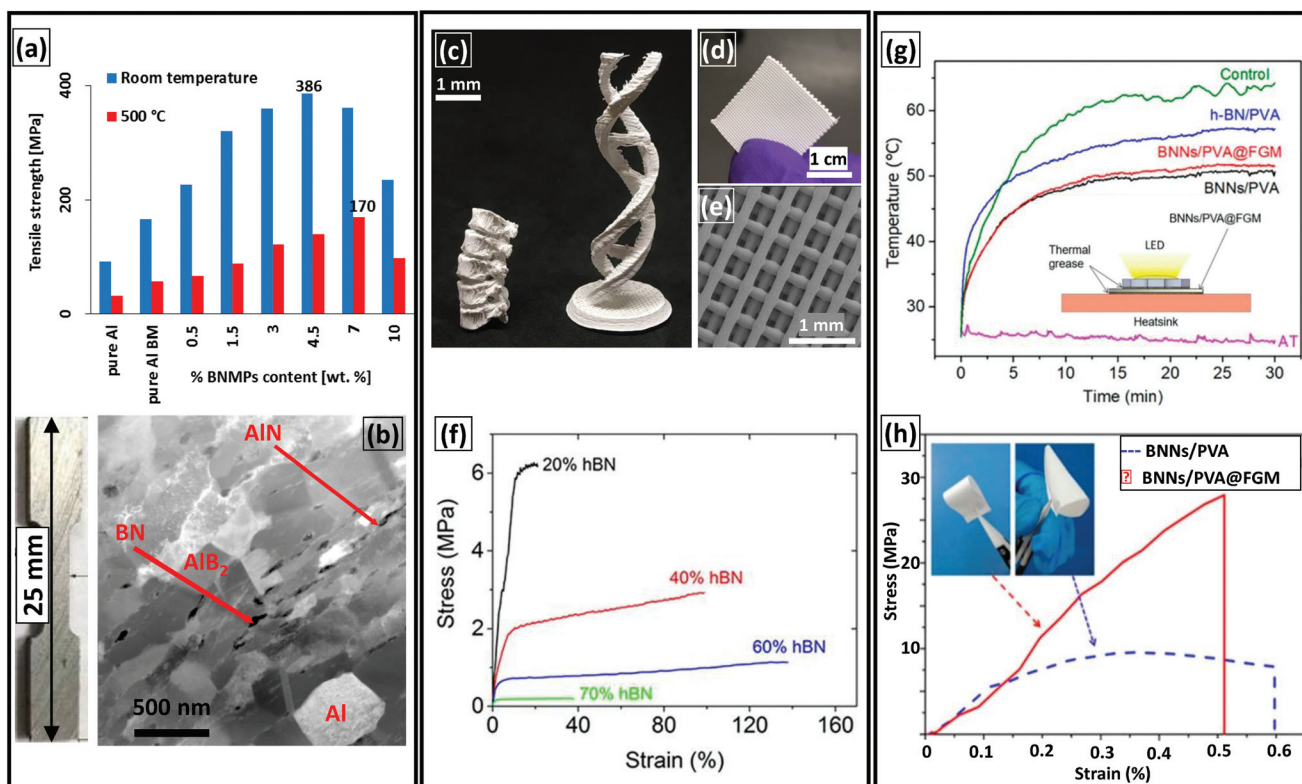


Fig. 7 (a) Relationship between ultimate tensile strength at room temperature (blue) and at 500 °C (red) and a BN phase content in Al/BN composites; (b) photo of a sample prepared for a tensile test and HAADF image of an Al/BN composite;⁸⁷ (c) photograph of small lumbar spine replica that were 3D printed using a 60% vol. *h*-BN nanocomposite ink;⁸⁸ (d–e) photograph and scanning electron micrographs of a 3D printed scaffold with 40% vol. *h*-BN;⁸⁸ (g) temperature variation of the working LED chip and configuration of a composite paper-based (BN content: 40 wt%) heatsink for LED;⁸⁹ (h) mechanical performance of the BNNs/PVA and BNNs/PVA@FGM composite papers;⁸⁹ the inset shows photos of highly flexible papers; (a) and (b) reprinted with permission from ref. 87. Copyright 2016 Elsevier. (c), (d), (e) and (f) Reprinted with permission from ref. 88. Copyright 2018 American Chemical Society. (g) and (h) reprinted with permission from ref. 89. Copyright 2018 American Chemical Society.

alignment approach was proposed by Yu *et al.*¹⁰⁴ In their composite films, the 2D *h*-BN platelets were hierarchically arranged in polyurethane due to hot-pressing induced alignment in the framework. Composite film with 95 wt% of *h*-BN exhibited a 264-fold increase in thermal conductivity (50.3 W m⁻¹ K⁻¹) compared to pure polyurethane. Adding BNNSSs to thermoplastic polyamide-imide led to a thermal conductivity enhancement of more than 400%.⁹⁷ This effect was attributed to the construction of 3D interconnected network. Hybrid elastomeric polyurethane-based composites with two-dimensional MoS₂/*h*-BN nanofillers demonstrated an even higher increase in thermal conductivity (~750%).⁹⁹ The addition of *h*-BN-reduced graphene oxide hybrids into epoxy resins was shown to improve the thermal conductivity, dielectric properties, and energy storage performance.⁹⁵ Enhanced thermal conductivity of polymeric composites with Ag NP-deposited BNNSSs was attributed to the decreased thermal resistance between BNNSSs with the bridging connections by Ag NPs.⁹⁶ *h*-BNNSSs were also used to fabricate a composite paper with in-plane thermal conductivity and high mechanical strength.⁸⁹ The composite paper was produced by simple method of spraying the BNNSSs and poly(vinyl alcohol) solution on a fiberglass mesh.

BNNSSs were utilized to provide self-healing ability to poly (*p*-phenylene benzobisoxazole) fibers under Xenon lamp irradiation.¹⁰⁵ The BNNSSs were immobilized onto PBO fibers using facile polydopamine chemistry. Guiney *et al.*⁸⁸ produced a high-content BN-polymer nanocomposite ink for 3D printing. The presence of *h*-BN improved mechanical strength and enhanced thermal conductivity, which had a positive effect on the 3D printing process.

7. BN nanostructures as perspective additives to reduce friction and wear

Control of friction and wear is a widely recognized problem that is related to a broad range of material applications from machine and engine components, to medical devices and micro- and nano-electromechanical systems. Nanoparticles are of interest due to their ability to be used as solid lubricants, additives in liquid lubricants, such as oils, and in nanocomposites (Fig. 8). A complete review of the tribological performance of NPs as lubricating oil additives was recently completed by Gulzar *et al.*¹⁰⁸ The most important challenges are to

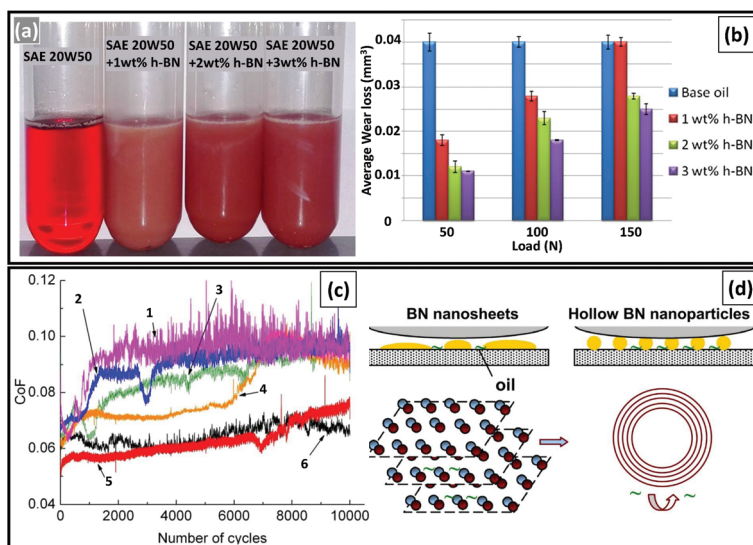


Fig. 8 (a) 20W50 engine oil with *h*-BN nanoparticles and (b) wear loss versus load on cylinder liner at a sliding velocity of 0.03 ms^{-1} at various concentrations of *h*-BN as an additive in 20W50;¹⁰⁶ (c) coefficient of friction measured during sliding of two 100Cr6 surfaces (pin-on-plate configuration in multipass reciprocating mode) in the presence of different suspensions: 1 – PAO6, 2 – PAO6 + 0.01P*–BNNPs, 3 – PAO6 + 0.1P–BNNPs, 4 – PAO6 + 0.1H*–BNNPs, 5 – PAO6 + 0.01N*–BNNPs, 6 – PAO6 + 0.1N–BNNPs;¹⁰⁷ and (d) schematics of possible wear mechanisms using PAO6 + BNNPs lubricants with BN nanosheet-based (left) and hollow spherical BN nanobearings;¹⁰⁷ (a) and (b) reprinted with permission from ref. 106. Copyright 2016 Wiley. (c) and (d) Reprinted with permission from ref. 107. Copyright 2018 Elsevier. *P, H and N refer to “pompon-like NPs, globular NPs formed by numerous *h*-BN nanosheets and hollow NPs with smooth surface, respectively.

maintain dispersion stability for a long time and to achieve reduced friction at a low particle concentration. This decreases the oil viscosity. As a potential solid lubricant, *h*-BN possesses a combination of advantageous properties, such as low density of surface dangling bonds, high mechanical strength, good thermal conductivity, as well as excellent chemical and thermal stability. BN nanostructures can be obtained in different morphologies, such as nanosheets and spherical nanoparticles. Nanosheets are of particular interest for advanced superlubricity systems. Adding of only 0.1 wt% of *h*-BNNPs to PAO6 oil permitted to noticeably decrease the friction coefficient from 0.1 to 0.06 and significantly reduce the wear rate of two sliding 100Cr6 surfaces.¹⁰⁷ *In situ* TEM compression tests demonstrated that during deformation, the contact area between the BNNPs and a counterpart material became flat with a great degree of alignments of the basal hexagonal BN planes parallel to the friction direction.¹⁰⁷ In case of a weak van der Waals force, two adjacent layers can be easily moved relative to each other resulting in low friction. Compressive tests on hollow BNNPs showed that they could withstand high contact pressure of about 1.0 GPa and mostly restored their initial shape after unloading, hereby providing low friction via a rolling mechanism.¹⁰⁹ Recent results demonstrated a great potential of using BNNPs as an additive for improving the load-carrying ability of different liquid lubricants (SAE 15W-40⁹ and SAE 20W50¹⁰⁶ diesel engine oils, environmentally friendly crude jatropha oil,¹¹⁰ and paraffin¹¹¹), particularly under high applied loads.^{9,106} The dispersion of *h*-BNNPs in liquid lubricants was reported to reduce friction by 30–75%.^{106,110} Owing to a layered structure, *h*-BN is

considered as one of the suitable additives for the improvement in wear and friction of metal matrix composites and polymers. For example, BNNPs enhanced wear resistance of AA6082/TiB₂ aluminum composites while acting as a solid lubricant and forming a tribofilm.¹¹¹ After *h*-BN addition to poly(aryletherketone) a wear rate was reduced approximately 22 times compared to the pure matrix.¹¹²

8. Theoretical simulations supporting BN-based nanoparticle fabrications and applications

Theoretical simulations can significantly stimulate the development, fabrication, and application of BNNPs and BN-based NHs (Fig. 9). McLean *et al.*¹¹⁴ reviewed recent advances in the application of chemical vapor deposited BN nanomaterials and highlighted the importance of density functional theory (DFT) calculations to uncover the *h*-BN growth mechanisms. Based on DFT, *ab initio* molecular dynamics (MD), and lattice dynamics calculations Rajan *et al.*¹¹⁵ developed a classical force field approach enabling modeling of *h*-BN nanostructures. Using DFT, Fu *et al.*¹¹⁶ showed that N-terminating zigzag (ZZ) edges are the most stable for triangular *h*-BN nanosheets. According to Zhao *et al.*,¹¹⁷ the formation of non-hexagonal rings is energetically not preferred and both ZZ edges are more stable than the armchair (AC) edge on the surface of BN/Cu(111), BN/Ni(111) and BN/Rh(111) catalysts. By applying the theory of Wulff construction, the equilibrium

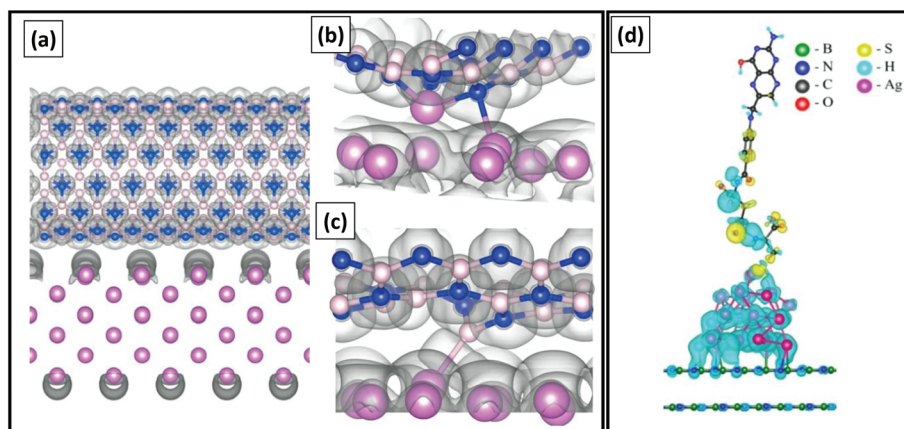


Fig. 9 (a) Electron density plotted as an isosurface for the adsorption of BNNT on Al: a pristine BNNT on (110) Al sheet; (b, c) BNNT with a B-vacancy and an N-vacancy on a (001) Al sheet, (c), respectively. The ivory and blue spheres indicate B and N atoms, respectively. Aluminum atoms are shown in pink;¹¹³ (d) distribution of spatial charge density between FA-Cyst-Ag/BNNPs (α -COOH) and corresponding freestanding parts. The loss and gain of charge are denoted by yellowish and bluish colors, respectively. The boron, nitrogen, carbon, oxygen, sulfur, hydrogen and silver atoms are marked in green, blue, grey, red, yellow, cyan and purple colors, respectively.⁸¹ (a), (b) and (c) Reprinted with permission from ref. 113. Copyright 2018 American Chemical Society. (d) Reprinted with permission from ref. 81. Copyright 2017 American Chemical Society.

shape of BN domains was predicted. Specific orientation relationships arising from the weak B–N–Cu interactions at the *h*-BN edge were shown to prevent reconstruction of the Cu (111) substrate.¹¹⁸ Relationship between CVD process parameters and the atomic structure of *h*-BN islands nucleated on Cu(111) and Ni(111) substrates was elucidated by Zhang *et al.*¹¹⁹ Depending on the B chemical potential, either triangular *h*-BN islands enclosed by N-terminated ZZ edges (low potential), or B-terminated and N-terminated Klein edges (high potential) were observed. Krstic *et al.*¹²⁰ performed classical MD simulation of BN nanostructure growth in hot, high pressure gas. It was demonstrated that four best precursors (radical BN, the closed-shell borazine ($B_3N_3H_6$) molecule, a mix of BN radicals and H atoms in a 4 : 1 ratio, and iminoborane (radical HBNH)) are able to create significant number of BN clusters in the form of flakes, BN cages, *t*-BNs, and BNNTs with the smallest number of defects. Importantly, the widely accepted theory of the “root growth” was not confirmed. Reimers *et al.*¹²¹ compared the results of DFT and *ab initio* simulations of the V_{NCB} defects in *h*-BN and drew attention to the fact that, for accurate description, the model should include one or more rings of atoms outside the ring that minimally describes the defect. Using MD simulations it was demonstrated that the presence of holes in BNNTs deteriorates their mechanical properties.¹²²

Classical MD simulations were undertaken to understand stable aqueous dispersions of BNNTs obtained by the sonication assisted exfoliation of *h*-BN powders in water without use of a stabilizer.¹²³ It was demonstrated that the dispersions are stabilized by electrostatic interactions between positively charged BNNTs that are formed during delamination. MD simulations of an implantation process of Ag ions into BNNPs were carried out by Firestein *et al.*²⁶ to understand the formation of Ag/BN NHs.

DFT calculations of the interface strength between metal matrix and reinforcing phase were engaged to predict new MMCs with enhanced mechanical properties or to support the experimental data. In case of structural materials, the recent data include BN–Mg¹²⁴ and BN–Al¹²⁵ interfaces. *Ab initio* and analytical potential calculations were carried out to uncover the mechanical properties of Al-based nanocomposites reinforced with BN nanoribbons.¹²⁶ It was demonstrated that active chemical edges of the ribbons create strong chemical bonding between the fillers and metal matrix and yield critical shear stress in the GPa range. Using classical MD methods, structural transformations in Al/BN composite nanomaterials during their fabrication were described. The formation of the rigid interfaces between Al and either AlN or AlB₂ phases ((111)_{Al}//(0001)_{AlN} with high binding energy and (111)_{Al}//(0001)_{AlB₂} with high critical shear stress values) was reported to be responsible for the high composite strength.⁹¹ Quantum chemical calculations demonstrated that Al binding to BN nanostructures was strongly enhanced at defects on the BN surface.¹¹³ Thus it was proposed that the commonly observed formation of AlN and AlB₂ phases at the Al/BN interface was due to N- or B-vacancy defects within BN. Recent review by Verma *et al.*¹²⁷ encompassed different types of interatomic potentials that can be used for modeling of PMCs reinforced with *h*-BN nanostructures. The high *h*-BN/polymer bonding was reported to be achieved mainly due to the high surface-to-volume ratio of BN derivatives that tends to stretch the polymer chains and pack them along the BN nanofiller surface leading to a higher densification in vicinity of filler relative to the bulk.

The relative stability and melting of cubic-BN (*c*-BN) nanoparticles of varying shapes and sizes was studied by Lee *et al.*¹²⁸ using classical MD simulation. The results indicated that the melting point of *c*-BN nanoparticles is size-dependent

and the size effect on melting is significant for small *c*-BN nanoparticles with a total number of atoms <5000. MD simulations also predicted that melting of *c*-BN nanoparticles is accompanied by phase segregation, resulting in formation of a boron-core nitrogen-shell structure, which was also supported by experiments.

Detailed energetic analysis of the atomic structure and stability of nanoconjugates using DFT calculations can shed light on the folic acid to BNNPs binding mechanism, which is important for targeted drug delivery.⁸¹ In addition, theoretical studies were performed for getting insights into nature of interactions between BNNPs and antibiotics using DFT formalism.¹²⁹ In contrast to earlier results indicating the formation of covalent bonding,¹³⁰ the interaction of antibiotics with BN nanomaterials was proposed to occur *via* van der Waals forces between the fluoroquinolone and BNNPs and is accompanied with a release of energy at the absence of charge transfer between the nanomaterial and the drug.

The catalytic activity of NHs can be theoretically analyzed using DFT calculations. Using DFT theory Lu *et al.*¹³¹ suggested that CO oxidation of Ag single atoms supported on *h*-BNNPs can proceed by the termolecular Eley-Rideal mechanism in a broad temperature range. To explain the correlation between the oxidized state of BNNPs and the amount of Ag NPs on their surfaces, the adhesion energy of the (111)Ag with (0001)h-BN and (100)B₂O₃ surfaces was determined by DFT calculations.⁵¹ Results indicated that, in contrast to non-wetted *h*-BN surface (the adhesion energy of *h*-BN with Ag is 0.04 eV Å⁻²), metallic Ag bound well to B₂O₃ (adhesion energy 0.17 eV Å⁻²) with the formation of a covalent bond at the interface. The electrocatalytic activities of *h*-BN/Ni, *h*-BN/Co, and *h*-BN/Cu interfaces were investigated for CO₂ reduction by the first-principles DFT.¹³² On the basis of the free-energy diagrams, it was predicted that *h*-BN/Ni and *h*-BN/Co should have very good electrocatalytic activities toward CO₂ reduction to HCOOH. The mechanism behind is an electron transfer from the metal to *h*-BN leading to a unique chemical reactivity of the *h*-BN/metal interface. Systematic studies of Ni atoms on defective *h*-BN nanosheets and their application for the reversible hydrogen storage at room temperature was carried out by Zhou *et al.* using the DFT simulations.¹³³ The defective *h*-BNNPs were shown to improve the binding energy of Ni atoms. Along three types of defects studied (Stone-Wales defect, B- or N vacancy), only the Ni-decorated V_N nanosheet showed a desirable adsorption energy in the range of -0.40–0.51 eV, which fits the requirement for H₂ storage.

Theoretical studies were also carried out to predict the electronic properties of BN monoatomic sheets after oxygen doping and/or functionalization,¹³⁴ to uncover the compression process of hollow BNNPs,¹⁰⁹ as well as to determine the interlayer shear force between *h*-BN/*h*-BN and graphene (G)/*h*-BN.¹³⁵ Using first-principle calculations, Guo *et al.*¹³⁶ studied the spin-dependent electronic transport in *h*-BN nanoribbons with edge defects and revealed a dual spin filler effect in which the direction of current spin polarization is switched by the defect.

9. Final remarks and future developments

Several recent studies were focused on further uncovering the unusual properties of BN nanostructures. Ziegler *et al.*¹³⁷ discovered bright, stable, visible-wavelength single-photon emitter in a nanometer-scale BN material that is ball-like, 0D BN allotrope. These emitters are active at room temperature and in air and are stable over many days. Brown *et al.*¹³⁸ demonstrated the possibilities of photothermal induced resonance technique for direct observation of dark hyperbolic modes in *h*-BN nanostructures.

There are many other exciting applications of BN nanostructures and their nanohybrids. Due to the enhanced thermal stability, Au/BN^{139,140} and Ag/BN¹⁴¹ NHs can be used as SERS substrates. The detection of chemical or biological species by a SERS sensor is based on the enhancement of a Raman signal upon the adsorption of a sensing species.¹⁴² Gao *et al.*¹⁴⁰ combined Au NP arrays with chemically exfoliated few-layer BNNPs to form Au/BN composites with SERS. The underlining physical mechanism for SERS was proposed to be a charge transfer and plasmonic coupling of Au NPs with BNNPs. BN/Ag NHs were reported to capture the pollutants from an aqueous solution rapidly and also revealed enhanced SERS activity of 10⁻⁹ M.¹⁴³ The pores of BN protect the Ag NPs from aggregation and enable BN/Ag a stable and recyclable SERS substrate.

BN nanostructures can be used for the development of miniature electronic, optoelectronic, magnetic, energy storage, and biological devices. For example, a high frequency magnetic composite consisting of FeCo core and BN shell that simultaneously exhibited high electrical resistivity and magnetic permeability was reported.¹⁴⁴ A novel electrochemical sensor based on BN flakes was recently fabricated by Li *et al.*¹⁴⁵ The developed sensor exhibited excellent electrocatalytic activities toward ascorbic acid, dopamine and uric acid. BN-Pt composites were reported to exhibit a good amperometric response toward the reduction and oxidation of H₂O₂, which allowed it to be utilized as a bioplatform for glucose biosensor.¹⁴⁶ Hydroxylated BNNPs were doped into an organically modified silicate matrix through a facile sol-gel process to form ultra-broadband optical limiting solid transparent materials for optoelectronic devices.¹⁴⁷ Layered nanocomposites consisting of BNNPs and regenerated cellulose were prepared from a NaOH/urea aqueous solution and confirmed to be promising energy storage devices.¹⁴⁸ Their energy storage density of 4.1 J cm⁻³ surpassed existing commercial dielectric polymers. *h*-BNNPs were utilized to create rolled up magnetic nanoscrolls with potential applications in areas such as catalysis, thermoelectrics and solar conversion.¹⁴⁹ *h*-BN nanoscrolls decorated with magnetic Au@Fe₃O₄ NPs had both optical and magnetic components and, therefore, provide a tunable magnetization compared to that of the Fe₃O₄ nanocomposites and prevent magnetic coupling between NPs.

Due to high adsorbing capacity for gas molecules BNNPs are promising materials for gas sensors because of their gra-

phene-like 2D layered structures with a wide band gap.¹⁵⁰ 2D *h*-BN nanoflakes were utilized to fabricate BN/polymer humidity sensors.¹⁵¹ BN nanostructures were used to make the sensing layer that provides the secondary path for ionic current between different energy levels of BNNSs. A BN quantum dots-based turn-off sensor showed potential prospects for rapid and selective detection of 2,4,6-trinitrophenol (TNP) in natural water.¹⁵² BNNSs were used as a buffer layer in graphene/N-functionalized graphene quantum dot hybrid broadband photodetector.¹⁵³ The BN nanosheet buffer layer facilitated the separation and transport of photoexcited carriers from the diaminonaphthalene-functionalized graphene quantum dots photon absorber to graphene. Recently, the luminescence properties of exfoliated thin *h*-BN flakes were studied.¹⁵⁴ The obtained results indicated a thickness-dependence of luminescence that further confirmed unique properties of *h*-BN.

As a final remark we may also give several most recent selected and representative examples, which further demonstrate extremely wide opportunities of BNNPs and keep the room open for further findings and developments in this quickly developing field: (i) two-dimensional layered *h*-BN insulator was used for surface passivation on semiconductor TiO₂ to improve the material electronic quality and performance of the resulting dye-sensitized solar cell,¹⁵⁵ (ii) *h*-BN was utilized for fabrication of new neutron shielding materials based on high density polyethylene with different amounts of *h*-BN and Gd₂O₃ NPs,¹⁵⁶ (iii) due to high thermal conductivity and excellent insulation properties, BNNSs were added to water to make a cooling nanofluid with high thermal conductivity (increase by almost 300% in comparison with pure water).¹⁵⁷

Conflicts of interest

There are no conflicts to declare.

Acknowledgements

Authors thank a financial support from the Ministry of Education and Science of the Russian Federation (D. G. acknowledges the Increase Competitiveness Program of NUST "MISiS" No. K2-2017-082 and D. V. S. is grateful for the State task No. 11.937.2017/ПЧ). D. G. is also grateful to the Australian Research Council Laureate Fellowship FL160100089 and the QUT grants no. 322170-0355/51 and 322170-0348/07.

References

- 1 T. Li, L. Wang, K. Zhang, Y. Xu, X. Long, S. Gao, R. Li and Y. Yao, *Small*, 2016, **12**, 4960–4965.
- 2 Y. Xue, X. Zhou, T. Zhan, B. Jiang, Q. Guo, X. Fu, K. Shimamura, Y. Xu, T. Mori, P. Dai, Y. Bando, C. Tang and D. Golberg, *Adv. Funct. Mater.*, 2018, **28**, 1801205.
- 3 Z. He, C. Kim, T. H. Jeon and W. Choi, *Appl. Catal., B*, 2018, **237**, 772–782.
- 4 H. Wang, W. Wang, H. Wang, F. Zhang, U. Li and Z. Fu, *Ceram. Int.*, 2018, **44**, 12216–12224.
- 5 J. Xiong, J. Luo, L. Yang, J. Pang, W. Zhu and H. Li, *J. Ind. Eng. Chem.*, 2018, **64**, 383–389.
- 6 G. Liu, Z. Zhang, C. Yan, Y. Wang, X. Ma, P. Gao and Y. Feng, *J. Chemosphere*, 2018, **207**, 534–542.
- 7 J. Li, L. Gan, S. Mateti, W. Lei, Y. Chen and J. Yang, *Eur. Polym. J.*, 2018, **104**, 57–63.
- 8 M. Rivera, R. Velazquez, A. Aldabahi, A. F. Zhu and P. X. Feng, *J. Phys. D: Appl. Phys.*, 2018, **51**, 045102.
- 9 M. I. H. C. Abdullah, M. F. B. Abdollah, N. Tamaldin, H. Amiruddin and N. R. M. Nuri, *Ind. Lubr. Tribol.*, 2016, **68**, 441–445.
- 10 N. R. Muthu, S. Rajashabala and R. Kannan, *Renewable Energy*, 2016, **85**, 387–394.
- 11 K. Zhang, Y. Feng, F. Wang, Z. Yang and J. Wang, *J. Mater. Chem. C*, 2017, **5**, 11992–12022.
- 12 S. Kalay, Z. Yilmaz, O. Sen, M. Emanet, E. Kazanc and M. Culha, *Beilstein J. Nanotechnol.*, 2015, **6**, 84–102.
- 13 A. Pakdel, Y. Bando and D. Golberg, *Chem. Soc. Rev.*, 2014, **43**, 934–959.
- 14 V. Salles and S. Bernard, *Nanomater. Nanotechnol.*, 2016, **6**, 1.
- 15 A. T. Matveev, K. L. Firestein, A. E. Steinman, A. M. Kovalskii, I. V. Sukhorukova, O. I. Lebedev, D. V. Shtansky and D. Golberg, *J. Mater. Chem. A*, 2015, **3**, 20749–20757.
- 16 W. Han, Z. Ma, S. Liu, C. Ge, L. Wang and X. Zhang, *Ceram. Int.*, 2017, **43**, 10192–10200.
- 17 W. Han, J. Wang, S. Liu, C. Ge, S. Cao, B. Song, J. Wang and X. Zhang, *Ceram. Int.*, 2017, **43**, 3569–3575.
- 18 W. Han, L. Wang, R. Zhang, C. Ge, Z. Ma, Y. Yang and X. Zhang, *Eur. J. Inorg. Chem.*, 2017, 5466–5474.
- 19 Q. Lu, Q. Zhao, T. Yang, C. Zhai, D. Wang and M. Zhang, *ACS Appl. Mater. Interfaces*, 2018, **10**, 12947–12953.
- 20 A. M. Kovalskii, A. T. Matveev, O. I. Lebedev, I. V. Sukhorukova, K. L. Firestein, A. E. Steinman, D. V. Shtansky and D. Golberg, *CrystEngComm*, 2016, **18**, 6689–6699.
- 21 Q. Li, C. Huo, K. Yi, L. Zhou, L. Su and X. Hou, *Sens. Actuators, B*, 2018, **260**, 346–356.
- 22 B. Zhong, X. Zhang, L. Xia, Y. Yu and G. Wen, *Mater. Des.*, 2017, **120**, 266–272.
- 23 R. Geng, Y. Xu, S. E. C. Li, C. Yu, T. Li, X. Long, W. Gong, J. Wu and Y. Yao, *Ceram. Int.*, 2018, **44**, 14228–14235.
- 24 J. Liang, J. Lin, R. Li, Q. Song, Y. Fang, C. Yu, H. Luo, Z. Liu, C. Tang and Y. Huang, *Ceram. Int.*, 2017, **43**, 15402–15409.
- 25 K. L. Firestein, A. E. Steinman, D. V. Leybo, A. T. Matveev, A. M. Kovalskii, I. V. Sukhorukova, P. V. Slukin, N. K. Fursova, S. G. Ignatov, D. Golberg and D. V. Shtansky, *Beilstein J. Nanotechnol.*, 2018, **9**, 250–261.

- 26 K. L. Firestein, D. G. Kvashnin, A. N. Sheveyko, I. V. Sukhorukova, A. M. Kovalskii, A. T. Matveev, O. I. Lebedev, P. B. Sorokin, D. Golberg and D. V. Shtansky, *Mater. Des.*, 2016, **98**, 167–173.
- 27 G. Gao, A. Mathkar, E. P. Martins, D. S. Calvão, D. Gao, P. A. da Silva Autreto, C. Sun, L. Cai and P. M. Ajayan, *J. Mater. Chem.*, 2014, **2**, 3148–3154.
- 28 L. Fu, G. Chen, N. Jiang, J. Yu, C.-T. Lin and A. Yu, *J. Mater. Chem. A*, 2016, **4**, 19107–19115.
- 29 H. Shen, C. Duan, J. Guo, N. Zhao and J. Xu, *J. Mater. Chem.*, 2015, **3**, 16663–16669.
- 30 S. K. Singhal, V. Kumar, K. Stalin, A. Choudhary, S. Teotia, G. B. Reddy, R. B. Mathur, S. P. Singh and R. Pasricha, *Part. Part. Syst. Charact.*, 2013, **30**, 445–452.
- 31 C. Huang, Q. Liu, W. Fan and X. Qiu, *Sci. Rep.*, 2015, **5**, 16736.
- 32 D. Fan, X. Lv, J. Feng, S. Zhang, J. Bai, R. Lu and J. Liu, *Int. J. Hydrogen Energy*, 2017, **42**, 11312–11320.
- 33 W. Wang, J. Lin, C. Xing, R. Chai, S. Abbas, T. Song, C. Tang and Y. Huang, *Ceram. Int.*, 2017, **43**, 6371–6376.
- 34 F. Cao, Y. Ding, L. Chen and C. Zhang, *Nanoscale*, 2013, **5**, 10000–10006.
- 35 J. Zhou, Q. Wang, Q. Sun and P. Jena, *Phys. Rev. B: Condens. Matter Mater. Phys.*, 2010, **81**, 085442.
- 36 J. Zeng, K.-Q. Chen and C. Q. Sun, *Phys. Chem. Chem. Phys.*, 2012, **14**, 8032–8037.
- 37 D. Xu, Y.-J. Liu, J.-X. Zhao, Q.-H. Cai and X.-Z. Wang, *J. Phys. Chem. C*, 2014, **118**, 8868–8876.
- 38 L.-Y. Feng, Y.-J. Liu and J.-X. Zhao, *J. Power Sources*, 2015, **287**, 431–438.
- 39 S. Lin, J. Huang and X. Ye, *Appl. Surf. Sci.*, 2014, **320**, 237–243.
- 40 K. Uosaki, G. Elumalai, H. Noguchi, T. Masuda, A. Lyalin, A. Nakayama and T. Taketsugu, *J. Am. Chem. Soc.*, 2014, **136**, 6542–6545.
- 41 W. S. Zhu, B. L. Dai, P. W. Wu, Y. H. Chao, J. Xiong, H. P. Li and H. M. Li, *Chem. Eng.*, 2015, **3**, 186–194.
- 42 X. Liu, T. Duan, Y. Sui, C. Meng and Y. Han, *RSC Adv.*, 2014, **4**, 38750–38760.
- 43 G. Min, A. Lyalin and T. Taketsugu, *J. Phys. Chem. C*, 2012, **116**, 9054–9062.
- 44 M. Gao, A. Lyalin and T. Taketsugu, *Int. J. Quantum Chem.*, 2013, **113**, 443–452.
- 45 G. Elumalai, H. Noguchi, H. C. Dinh and K. Uosaki, *J. Electroanal. Chem.*, 2018, **819**, 107–113.
- 46 L. Fu, G. Chen, N. Jiang, J. Yu, C.-T. Lin and A. Yu, *J. Mater. Chem. A*, 2016, **4**, 19107–19115.
- 47 Q. Li, W. Luo, L. Su, J. Chen, K.-C. Chou and X. Hou, *RSC Adv.*, 2016, **6**, 92748–92753.
- 48 H. Goto, A. Takagaki, R. Kikuchi and S. T. Oyama, *Appl. Catal., A*, 2017, **548**, 122–127.
- 49 A. Harley-Trochimczyk, T. Pham, J. Chang, E. Chen, M. A. Worsley, A. Zettl, W. Mickelson and R. Maboudian, *Adv. Funct. Mater.*, 2016, **26**, 433–439.
- 50 H. Shen, C. Duan, J. Guo, N. Zhao and J. Xu, *J. Mater. Chem.*, 2015, **3**, 16663–16669.
- 51 A. S. Konopatsky, K. L. Firestein, D. V. Leybo, Z. I. Popov, K. V. Larionov, A. E. Steinman, A. M. Kovalskii, A. T. Matveev, A. Manakhov, P. B. Sorokin, D. Golberg and D. V. Shtansky, *Catal. Sci. Technol.*, 2018, **8**, 1652–1662.
- 52 J. Pang, Y. Chao, H. Chang, H. Li, J. Xiong, Q. Zhang, G. Chen, J. Qian, W. Zhu and H. Li, *ACS Sustainable Chem. Eng.*, 2018, **6**, 49–4957.
- 53 X. J. Yang, L. L. Li, W. L. Sang, J. L. Zhao, X. X. Wang, C. Yu, X. H. Zhang and C. C. Tang, *J. Alloys Compd.*, 2017, **693**, 642–649.
- 54 Q. Fu, Y. Meng, Z. Fang, Q. Hu, L. Xu, W. Gao, X. Huang, Q. Xue, Y. P. Sun and F. Lu, *ACS Appl. Mater. Interfaces*, 2017, **9**, 2469–2476.
- 55 Y. Wang, L. Shi, W. Lu, Q. Sun, Z. Wang, C. Zhi and A. H. Lu, *ChemCatChem*, 2017, **9**, 1363–1367.
- 56 X. Lv, J. Wang, Z. Yan, D. Jiang and J. Liu, *J. Mol. Catal. A: Chem.*, 2016, **418–419**, 146–153.
- 57 Y. Song, H. Xu, C. Wang, J. Chen, J. Yan, Y. Xu, Y. Li, C. Liu, H. Li and Y. Lei, *RSC Adv.*, 2014, **4**, 56853–56862.
- 58 C. Zhu, J. Zheng, L. Fang, P. Hu, Y. Liu, X. Cao and M. Wu, *J. Mol. Catal. A: Chem.*, 2016, **424**, 135–144.
- 59 J. Yan, J. Gu, X. Wang, Y. Fan, Y. Zhao, J. Lian, Y. Xu, Y. Song, H. Xu and H. Li, *RSC Adv.*, 2017, **7**, 25160–25170.
- 60 Y. Ide, F. Liu, J. Zhang, N. Kawamoto, K. Komaguchi, Y. Bando and D. Golberg, *J. Mater. Chem. A*, 2014, **2**, 4150–4156.
- 61 Y. Ide, K. Nagao, K. Saito, K. Komaguchi, R. Fiji, A. Kogure, Y. Sugahara, Y. Bando and D. Golberg, *Phys. Chem. Chem. Phys.*, 2016, **18**, 79–83.
- 62 D. Liu, M. Zhang, W. Xie, L. Sun, Y. Chen and W. Lei, *Appl. Catal., B*, 2017, **207**, 72–78.
- 63 B. Singh, G. Kaur, P. Singh, K. Singh, J. Sharma, M. Kumar, R. Bala, R. Meena, S. K. Sharma and A. Kumar, *New J. Chem.*, 2017, **41**, 11640–11646.
- 64 Y. Cao, M. Lu, J. Fang, L. Shi and D. Zhang, *Chem. Commun.*, 2017, **53**, 7549–7552.
- 65 M. Du, Q. Liu, C. Huang and X. Qiu, *RSC Adv.*, 2017, **7**, 35451–35459.
- 66 S. Yu, X. Wang, H. Pang, R. Zhang, W. Song, D. Fu, T. Hayat and X. Wang, *Chem. Eng. J.*, 2018, **333**, 343–360.
- 67 P. Chaturbedy, M. Ahamed and M. Eswaramoorthy, *ACS Omega*, 2018, **3**, 369–374.
- 68 M. D. Esrafili and N. Saeidi, *Appl. Surf. Sci.*, 2018, **444**, 584–589.
- 69 C. Huang, C. Chen, M. Zhang, L. Lin, X. Ye, S. Lin, M. Antonietti and X. Wang, *Nat. Commun.*, 2015, **6**, 7698.
- 70 J. Pang, Y. Chao, H. Chang, H. Li, J. Xiong, Q. Zhang, G. Chen, J. Qian, W. Zhu and H. Li, *ACS Sustainable Chem. Eng.*, 2018, **6**, 49–4957.
- 71 D. Farmanzadeh and N. A. Ardehjani, *Appl. Surf. Sci.*, 2018, **44**, 642–649.
- 72 R. Nie, R. Sang, X. Ma, Y. Zheng, X. Cheng, W. Li, L. Guo, H. Jin and Y. Wu, *J. Catal.*, 2016, **344**, 286–292.
- 73 Q. H. Weng, X. B. Wang, X. Wang, Y. Bando and D. Golberg, *Chem. Soc. Rev.*, 2016, **45**, 3989–4012.

- 74 M. M. Chen, D. Wei, W. Chu, T. Wang and D. G. Tong, *J. Mater. Chem.*, 2017, **5**, 17029–17039.
- 75 M. Ji, J. Xia, J. Di, Y. Liu, R. Chen, Z. Chen, S. Yin and H. Li, *Chem. Eng. J.*, 2018, **331**, 355–363.
- 76 I. V. Sukhorukova, I. V. Zhitnyak, A. M. Kovalskii, A. T. Matveev, O. I. Lebedev, N. A. Gloushankova, X. Li, D. Golberg and D. V. Shtansky, *ACS Appl. Mater. Interfaces*, 2015, **7**, 17217–17225.
- 77 I. Y. Zhitnyak, I. N. Bychkov, I. V. Sukhorukova, A. M. Kovalskii, K. L. Firestein, D. Golberg, N. A. Gloushankova and D. V. Shtansky, *ACS Appl. Mater. Interfaces*, 2017, **9**, 32498–32508.
- 78 S. Mateti, C. S. Wong, Z. Liu, W. Yang, Y. Li, L. H. Li and Y. Chen, *Nano Res.*, 2018, **11**, 334–342.
- 79 S. Feng, H. Zhang, T. Yan, D. Huang, C. Zhi, H. Nakanishi and X. D. Gao, *Int. J. Nanomed.*, 2016, **11**, 4573–4582.
- 80 P. Singla, N. Goel and S. Singhal, *Chem. Eng. J.*, 2016, **299**, 403–414.
- 81 E. S. Permyakova, I. V. Sukhorukova, L. Yu. Antipina, A. S. Konopatsky, A. M. Kovalskii, A. T. Matveev, O. I. Lebedev, D. V. Golberg, A. M. Manakhov and D. V. Shtansky, *J. Phys. Chem. C*, 2017, **121**, 28096–28105.
- 82 S. M. Sharker, M. A. Alam, M. C. Shill, G. M. S. Rahman and H. M. Reza, *Int. J. Pharm.*, 2017, **534**, 206–212.
- 83 X. Li, X. Wang, J. Zhang, N. Hanagata, X. Wang, Q. Weng, A. Ito, Y. Bando and D. Golberg, *Nat. Commun.*, 2017, **8**, 13936.
- 84 M. Nasr, L. Soussan, R. Viter, C. Eid, R. Habchi, P. Miele and M. Bechelany, *New J. Chem.*, 2018, **42**, 1250–1259.
- 85 T. Lu, L. Wang, Y. Jiang, Q. Liu and C. Huang, *J. Mater. Chem. B*, 2016, **4**, 6103–6110.
- 86 K. Nedunchezhian, N. Aswath, M. Thiruppathy and S. Thirugnanamurthy, *J. Clin. Diagn. Res.*, 2016, **10**, ZE01–ZE04.
- 87 K. L. Firestein, C. Shakti, A. E. Steinman, A. T. Matveev, A. M. Kovalskii, I. V. Sukhorukova, D. Golberg and D. V. Shtansky, *Mater. Sci. Eng., A*, 2017, **681**, 1–9.
- 88 L. M. Guiney, N. D. Mansukhani, A. E. Jakus, S. G. Eallace, R. N. Shah and M. C. Hersam, *Nano Lett.*, 2018, **18**, 3488–3493.
- 89 T. Wang, D. Ou, H. Liu, S. Jiang, W. Huang, X. Fang, X. Chen and M. Lu, *ACS Appl. Nano Mater.*, 2018, **1**, 1705–1712.
- 90 K. L. Firestein, A. E. Steinman, I. S. Golovin, J. Cifre, A. T. Matveev, A. M. Kovalskii, D. V. Shtansky and D. Golberg, *Mater. Sci. Eng., A*, 2015, **642**, 104–112.
- 91 A. E. Steinman, C. Shakti, K. L. Firestein, D. G. Kvashnin, A. M. Kovalskii, A. T. Matveev, P. B. Sorokin, D. Golberg and D. V. Shtansky, *Mater. Des.*, 2018, **141**, 88–98.
- 92 T. Semenic, J. Hu, S. Kraemer, R. Housley and O. Sudre, *J. Am. Ceram. Soc.*, 2018, 1–11, DOI: 10.1111/jace.15711.
- 93 X. F. Wu, Z. H. Zhao, Y. Sun, H. Li, Y. J. Wang, C. X. Zhang, X. D. Gong, Y. D. Wang, X. Y. Yang and Y. Liu, *J. Inorg. Organomet. Polym.*, 2017, **27**, 1142–1147.
- 94 J. Zhu, Y. Chen, J. Ren, D. Zhao and W. Liu, *Ceram. Int.*, 2018, **44**, 10604–10610.
- 95 T. Huang, X. Zeng, Y. Yao, R. Sun, F. Meng, J. Xu and C. Wong, *Nanoscale*, 2017, **7**, 23355–23362.
- 96 F. Wang, X. Zeng, Y. Yao, R. Sun, J. Xu and C.-P. Wong, *Sci. Rep.*, 2015, **6**, 19394.
- 97 F. Jiang, S. Cui, N. Song, L. Shi and P. Ding, *ACS Appl. Mater. Interfaces*, 2018, **10**, 16812–16821.
- 98 M. Salehirad, M. M. A. Nikje and L. Ahmadian-Alam, *Ind. Eng. Chem. Res.*, 2018, **57**, 1803–1814.
- 99 H. Ribeiro, J. P. C. Trigueiro, M. C. Lopes, J. J. Pedrotti, C. F. Woellner, W. M. Silva, G. G. Silva and P. M. Ajayan, *J. Appl. Polym. Sci.*, 2018, 46560.
- 100 J. Chen, X. Huang, Y. Zhu and P. Jiang, *Adv. Funct. Mater.*, 2017, **27**, 1604754.
- 101 M. Loeblein, S. H. Tsang, M. Pawlik, E. J. R. Phua, H. Yong, X. W. Zhang, C. L. Gan and E. H. T. Teo, *ACS Nano*, 2017, **11**, 2033–2044.
- 102 C. Yu, J. Zhang, Z. Li, W. Tian, L. Wang, J. Luo, Q. Li, X. Fan and Y. Yao, *Composites, Part A*, 2017, **98**, 25–31.
- 103 J. Zhang, X. Wang, C. Yu, Q. Li, Z. Li, C. Li, H. Lu, Q. Zhang, J. Zhao, M. Hu and Y. Yao, *Compos. Sci. Technol.*, 2017, **149**, 41–47.
- 104 C. Yu, W. Gong, W. Tian, Q. Zhang, Y. Xu, Z. Lin, M. Hu, X. Fan and Y. Yao, *Compos. Sci. Technol.*, 2018, **160**, 199–207.
- 105 Q. Shao, Z. Hu, X. Xu, L. Yu, D. Zhang and Y. Huang, *Appl. Surf. Sci.*, 2018, **440**, 1159–1165.
- 106 M. S. Charoo and M. F. Wani, *Lubr. Sci.*, 2017, **29**, 241–254.
- 107 A. V. Bondarev, A. M. Kovalskii, K. L. Firestein, P. A. Loginov, D. A. Sidorenko, N. V. Shvindina, I. V. Sukhorukova and D. V. Shtansky, *Ceram. Int.*, 2018, **44**, 6801–6809.
- 108 M. Gulzar, H. H. Masjuki, M. A. Kalam, M. Varman, N. W. M. Zulkifli, R. A. Mufti and R. Zahid, *J. Nanopart. Res.*, 2016, **18**, 223.
- 109 K. L. Firestein, D. G. Kvashnin, A. M. Kovalskii, Z. I. Popov, P. B. Sorokin, D. Golberg and D. V. Shtansky, *Nanoscale*, 2018, **10**, 8099–8105.
- 110 N. Talib, R. M. Nasir and E. A. Rahim, *J. Cleaner Prod.*, 2017, **147**, 360–378.
- 111 W. Han, Z. Ma, S. Liu, C. Ge, L. Wang and X. Zhang, *Ceram. Int.*, 2017, **43**, 10192–10200.
- 112 M. D. Joshi, A. Goyal, S. M. Patil and R. K. Goyal, *J. Appl. Polym. Sci.*, 2017, 44409.
- 113 C. Rohmann, V. I. Yamakov, C. Park, C. Fay, M. Hankel and D. J. Searles, *J. Phys. Chem.*, 2018, **122**, 15226–15240.
- 114 B. McLean, C. A. Eveleens, I. Mitchell, G. Webber and A. J. Page, *Phys. Chem. Chem. Phys.*, 2017, **19**, 26466–26494.
- 115 A. G. Rajan, M. S. Strano and D. Blankschtein, *J. Phys. Chem. Lett.*, 2018, **9**, 1584–1591.
- 116 X. Fu and R. Zhang, *Nanoscale*, 2017, **9**, 6734–6740.
- 117 R. Zhao, F. Li, Z. Liu, Z. Liu and F. Ding, *Phys. Chem. Chem. Phys.*, 2015, **17**, 29327–29334.
- 118 X. Song, J. Gao, Y. Nie, T. Gao, J. Sun, D. Ma, Q. Li, Y. Chen, C. Jin, A. Bachmatiuk, M. H. Rümmeli, F. Ding, Y. Zhang and Z. Liu, *Nano Res.*, 2015, **8**, 3164–3176.

- 119 Z. Zhang, Y. Liu, Y. Yang and B. I. Yakobson, *Nano Lett.*, 2016, **16**, 1398–1403.
- 120 P. S. Krstic, L. Han, S. Irle and H. Nakai, *Chem. Sci.*, 2018, **9**, 3803–3819.
- 121 J. R. Reimers, A. Sajid, R. Kobayashi and M. J. Ford, *J. Chem. Theory Comput.*, 2018, **14**, 1602–1613.
- 122 K. E. Eshkalak, S. Sadeghzadeh and M. Jalaly, *Comput. Mater. Sci.*, 2018, **148**, 170–181.
- 123 V. Arunachalam and S. Vasudevan, *J. Phys. Chem.*, 2018, **122**, 4662–4669.
- 124 D. G. Kvashnin, A. V. Krasheninnikov, D. V. Shtansky, P. B. Sorokin and D. Golberg, *Phys. Chem. Chem. Phys.*, 2016, **18**, 965–969.
- 125 A. V. Krasheninnikov, N. Berseneva, J. Enkovaara, T. Björkman, R. M. Nieminen, P. B. Sorokin, D. Kvashnin, D. Shtansky and D. Golberg, *J. Phys. Chem. C*, 2014, **118**, 26894–26901.
- 126 D. G. Kvashnin, M. Ghorbani-Asl, D. V. Shtansky, D. Golberg, A. V. Krasheninnikov and P. B. Sorokin, *Nanoscale*, 2016, **8**, 20080–20089.
- 127 A. Verma, A. Parashar and M. Packirisamy, *Wiley Interdiscip. Rev.: Comput. Mol. Sci.*, 2017, e1346.
- 128 H. F. Lee, K. Esfarjani, Z. Dong, G. Xiong, A. A. Pelegri and S. D. Tse, *ACS Nano*, 2016, **10**, 10563–10572.
- 129 P. Singla, N. Goel and S. Singhal, *Chem. Eng. J.*, 2016, **299**, 403–414.
- 130 S. Mukhopadhyay, S. Gowtham, R. H. Scheicher, R. Pandey and S. P. Karna, *Nanotechnology*, 2010, **21**, 165703–165709.
- 131 Z. Lu, P. Lv, S. Li, D. Ma and R. Wu, *Phys. Chem. Chem. Phys.*, 2017, **19**, 16795–16805.
- 132 G. Hu, Z. Wu, S. Dai and D. Jiang, *ACS Appl. Mater. Interfaces*, 2018, **10**, 6694–6700.
- 133 X. Zhou, W. Chu, Y. Zhou, W. Sun and Y. Xue, *Appl. Surf. Sci.*, 2018, **439**, 246–253.
- 134 Q. Weng, D. G. Kvashnin, X. Wang, O. Cretu, Y. Yang, M. Zhou, C. Zhang, D. M. Tang, P. B. Sorokin, Y. Bando and D. Golberg, *Adv. Mater.*, 2017, **29**, 1700695.
- 135 Y. Li, W. Zhang, B. Guo and D. Datta, *Acta Mech. Solida Sin.*, 2017, **30**, 234–240.
- 136 Y.-D. Guo, H.-F. Liu, H.-L. Zeng, X.-H. Yan and X.-C. Song, *Phys. Chem. Chem. Phys.*, 2018, **20**, 9241–9247.
- 137 J. Ziegler, A. Blaikie, A. Ftthalizadeh, D. Miller, F. S. Yasin, K. Williams, J. Mohrhardt, B. J. McMorran, A. Zettl and B. Alemán, *Nano Lett.*, 2018, **18**, 2683–2688.
- 138 L. V. Brown, M. Davanco, Z. Sun, A. Kretinin, Y. Chen, J. R. Matson, I. Vurgaftman, N. Sharac, A. J. Giles, M. M. Fogler, T. Taniguchi, K. Watanabe, K. S. Novoselov, S. A. Maier, A. Centrone and J. D. Caldwell, *Nano Lett.*, 2018, **18**, 1628–1636.
- 139 X. Yu, R. Cai, J. Jiao, Y. Fan, Q. Gao, J. Li, N. Pan, M. Wu and X. Wang, *J. Alloys Compd.*, 2018, **730**, 487–492.
- 140 W. Gao, Y. Zhao, H. Yin and H. Li, *Nanoscale*, 2017, **9**, 13004–13013.
- 141 G. Gao, A. Mathkar, E. P. Martins, D. S. Calvão, D. Gao, P. A. da Silva Autreto, C. Sun, L. Cai and P. M. Ajayan, *J. Mater. Chem.*, 2014, **2**, 3148–3154.
- 142 S. Schlücker, *Angew. Chem., Int. Ed.*, 2014, **53**, 4756–4795.
- 143 P. Dai, Y. Xue, X. Wang, Q. Weng, C. Zhang, X. Jiang, D. Tang, X. Wang, N. Kawamoto, Y. Ide, M. Mitome, D. Golberg and Y. Bando, *Nanoscale*, 2015, **7**, 18992–18997.
- 144 W. Zhang, K. Patel and S. Ren, *Nanoscale*, 2017, **9**, 13203–13208.
- 145 Q. Li, C. Huo, K. Yi, L. Zhou, L. Su and X. Hou, *Sens. Actuators, B*, 2018, **260**, 346–356.
- 146 Q. Li, W. Luo, L. Su, J. Chen, K. C. Chou and X. Hou, *RSC Adv.*, 2016, **6**, 92748–92753.
- 147 Z. Xie, Y. Wu, X. Sun, S. Liu, F. Ma, G. Zhao, X. Hao and S. Zhou, *Nanoscale*, 2018, **10**, 4276–4283.
- 148 J. Lao, H. Xie, Z. Shi, G. Li, B. Li, G.-H. Hu, Q. Yang and C. Xiong, *ACS Sustainable Chem. Eng.*, 2018, **6**, 7151–7158.
- 149 D. Y. Hwang, K. H. Choi, J. E. Park and D. H. Suh, *Phys. Chem. Chem. Phys.*, 2017, **19**, 4048–4055.
- 150 P. K. Kannan, D. J. Late, H. Morgan and C. S. Rout, *Nanoscale*, 2015, **7**, 13293–13312.
- 151 M. Sajid, H. B. Kim, J. H. Lim and K. H. Choi, *J. Mater. Chem. C*, 2018, **6**, 1421–1432.
- 152 D. Peng, L. Zhang, F. F. Li, W. R. Cui, R. P. Liang and J. D. Qiu, *ACS Appl. Mater. Interfaces*, 2018, **10**, 7315–7323.
- 153 H. Tetsuka, A. Nagoya and S. I. Tamura, *Nanoscale*, 2016, **8**, 19677–19683.
- 154 L. Schué, B. Berini, A. C. Betz, B. Plaçais, F. Ducastelle, J. Barjon and A. Loiseau, *Nanoscale*, 2016, **8**, 6986–6993.
- 155 M. Shanmugam, R. Jacobs-Gedrim, C. Durcan and B. Yu, *Nanoscale*, 2013, **5**, 11275–11282.
- 156 S. G. İrim, A. A. Wis, M. A. Keskin, O. Baykara, G. Ozkoc, A. Avci, M. Doğru and M. Karakoc, *Radiat. Phys. Chem.*, 2018, **144**, 434–443.
- 157 X. Hou, M. Wang, L. Fu, Y. Chen, N. Jiang, C.-T. Lin, Z. Wang and J. Yu, *Nanoscale*, 2018, **10**, 13004–13010.